



2.9 to 1.9 Ga paleoalterations of Archean granitic basement of the Franceville basin (Gabon)

Idalina Moubiya Mouélé, Patrick Dudoignon, Abderrazak El Albani, Alain Meunier, Philippe Boulvais, François Gauthier-Lafaye, Jean-Louis Paquette, Hervé Martin, Michel Cuney

► To cite this version:

Idalina Moubiya Mouélé, Patrick Dudoignon, Abderrazak El Albani, Alain Meunier, Philippe Boulvais, et al.. 2.9 to 1.9 Ga paleoalterations of Archean granitic basement of the Franceville basin (Gabon). Journal of African Earth Sciences, 2014, 97, pp.244-260. 10.1016/j.jafrearsci.2014.04.027 . insu-01010619

HAL Id: insu-01010619

<https://insu.hal.science/insu-01010619>

Submitted on 20 Jun 2014

HAL is a multi-disciplinary open access archive for the deposit and dissemination of scientific research documents, whether they are published or not. The documents may come from teaching and research institutions in France or abroad, or from public or private research centers.

L'archive ouverte pluridisciplinaire **HAL**, est destinée au dépôt et à la diffusion de documents scientifiques de niveau recherche, publiés ou non, émanant des établissements d'enseignement et de recherche français ou étrangers, des laboratoires publics ou privés.

2.9 to 1.9 Ga paleoalterations of Archean granitic basement of the Franceville basin (Gabon).

Idalina Moubiya Mouélé^{a*}, Patrick Dudoignon^a, Abderrazak El Albani^a, Alain Meunier^a, Philippe Boulvais^b, François Gauthier-Lafaye^c Jean-Louis Paquette^{def}, Hervé Martin^{def}, Michel Cuney^g

^aUMR CNRS 7285, IC2MP, Bâtiment B35 – 5, avenue Albert Turpaine, 86022 Poitiers cedex, France

^bUMR 6118, département Géosciences, Université de Rennes, 35042 Rennes, France

^cUMR 7517 CNRS, Laboratoire d'Hydrologie et de Géochimie de Strasbourg, 1 rue Blessig 67082, Strasbourg cedex, France

^d Clermont Université, Université Blaise Pascal, Laboratoire Magmas et Volcans, BP 10448, F-63000 Clermont-Ferrand France

^e CNRS, UMR 6524, LMV, F-63038 Clermont-Ferrand France

^fIRD, R 163, LMV, F-63038 Clermont-Ferrand France

^gGeoRessources UMR 7359, BP 239, F-54506 Vandoeuvre les Nancy

1

2 *Corresponding author.

3 Address: Paleocirculation and Diagenesis in Archean basement, Franceville basin, Gabon

4

Abstract

The Archean granitoids in the Kiéné area, Gabon, are overlain by the Paleoproterozoic sediments of the Franceville basin (2.1 Ga). The basin is known for its high-grade uranium deposits among which some have been forming natural nuclear fission reactors. Most of the studies were dedicated to the FA-FB Paleoproterozoic sediments hosting these uranium deposits. Little is known on the Archean basement itself and specifically on the hydrous alteration events it experienced before and after the sediment deposition. The present work is focused on their petrographical, mineralogical and geochemical characterization. Dating the successive alteration events has been attempted on altered monazite crystals.

Rocks in different alteration states have been sampled from eight drill cores crosscutting the Archean - Paleoproterozoic unconformity. The Archean granitoids observed in the deepest levels exhibit typical petrographical features of a propylitic alteration while they are intensely illitized up to the unconformity. The propylitic alteration is mainly pervasive but the original texture of the granitoïds is conserved in spite of the formation of new minerals: Mg-chlorite, allanite and epidote forming a typical paragenesis. The illitic alteration is much more invasive near the unconformity. The illitization process leads to the replacement of feldspars and the corrosion of quartz crysals by an illitic matrix while the ferromagnesian minerals are pseudomorphosed by a Fe-chlorite + phengite+ hematite assemblage. The final fluid-rock interaction step is marked by fissural deposits of calcite and anhydrite. The $\delta^{13}\text{C}$ isotopic data show that the fissural carbonates precipitated from diagenetic fluids enriched carbon products deriving from the maturation of organic matter. The U-Pb isotopic analyses performed on monazite crystals have dated three distinct events: 3.0-2.9 Ga (magmatic), 2.6 Ga (propylitic alteration) and 1.9 Ga (diagenetic illitization). The calculation of geochemical mass balances suggests that the water – rock ratio during the propylitic alteration event was weak. On the contrary, it was much higher during the overprinted illitization which is characterized by an intense leaching of Na, Ca, Mg, Sr, REE and an enrichment in K, Rb,Cs.

Neither the petrographic features nor the geochemical data militate for an Archean weathering event (paleosol). In the present case, diagenetic fluids have percolated from the unconformity into the basement where they overprinted the illitization processes upon the previously propylitized rocks. These fluids were probably oxidant as they are also responsible of the U mobilization which led to the formation of the ore deposits close to the FA-FB interface.

- 5 **Keywords:** Archean, granitoid, hydrothermal, Paleoproterozoic, diagenesis, Francevillian

6

7

8

9 Introduction

10 The Archean basements have been frequently altered by multiple hydrothermal and/or
11 metamorphic events (Card, 1978; Murakami et al., 2011; Nedachi et al., 2005; Ohmoto, 1996;
12 Ohmoto and Kerrick, 1977). Additionally, in some cases, their erosion surface may conserve the
13 traces of weathering processes forming the so-called paleosols which are researched for their
14 paleo-atmospheric signification (Grandstaff et al., 1986; Holland, 1994; Maynard, 1992;
15 Mossman and Farrow, 1992; Ohmoto, 1996; Rye and Holland, 1998). At last, when overlain by
16 sedimentary deposits, the basement rocks may have suffered mineral reactions triggered by the
17 diagenetic fluid invasion (Mercadier et al., 2010). Because they are operating successively, all
18 these events may superimpose their effects in some places. Then, the genetic message carried by
19 the secondary minerals is difficult to interpret without an accurate petrographical study. This is
20 the backbone of the present work whose goal is to characterize the alteration events which have
21 affected the Archean basement under the Francevillian sedimentary series in Gabon. It was
22 globally affected by post-magmatic to metamorphic mineral reactions (Mathieu, 1999; Sère,
23 1996) but its alteration state near the unconformity is still poorly documented. Our work, focused
24 on that interface, was made possible thanks to several drill-holes which have been dug for
25 uranium ore exploration. The goal is to determine the origin of the secondary minerals and to date
26 their formation.

27

28 **2. Geological setting**

29 The Chaillu massif is located in the South Gabon which is Northeastern part of the Congo
 30 craton (Fig.1). It forms the granitic basement of the Paleoproterozoic sediments deposited in the
 31 Franceville basin. It is composed of different granitoid and orthogneiss bodies dated from 3.1 to
 32 2.5 Ga (Bouton et al., 2009; Caen-Vachette et al., 1988). These bodies are structurally and
 33 mineralogically heterogeneous because of two major plutonic events (Bouton et al., 2009;
 34 Chevallier et al., 2002; Prian and Johan, 1989; Thiéblemont et al., 2009; Thomas et al., 2001).
 35 The first one took place during the Mesoarchean (2928 ± 6 Ma to 2870 ± 5 Ma). It led to the
 36 intrusion of gray-coloured calc-alkaline granitoids belonging to typical a Archean Trondhjemite,
 37 Tonalite, Granodiorite suite (TTG) associated with migmatized quartz diorites (Thiéblemont et
 38 al., 2009). Locally, these rocks are cross-cut by diorite sills. The second period of magmatism
 39 belongs to the Neoarchean (2800 to 2550 Ma). It is characterized by the intrusion of alkaline to
 40 calc-alkaline pink to red magmatic rocks: syenites, syenogranites, granites and pegmatites
 41 (Thiéblemont et al., 2009).

42 The Franceville basin sedimentary series are composed of five unmetamorphosed formations,
 43 4000 m thick, sequentially labeled from FA at the base up to FE (Weber, 1968). The FA
 44 formation (500-1000 m thick) is directly deposited on the eroded surface of the Archean
 45 granitoids basement (Chaillu massif). It is essentially formed of conglomerates and sandstones
 46 typical of fluvio-deltaic deposits. Its upper part (Fig. 1) hosts the natural nuclear reactors of the
 47 Oklo, Okélobondo and Bangombé uranium ore bodies (Gauthier-Lafaye et al., 1996; Naudet,
 48 1991). The FA formation in the Kiéné area, exhibits a vertical granulometric evolution
 49 (conglomerate to sandstone and mudstone). The color of the sediments changes upwards from red
 50 to green to black (Gauthier-Lafaye, 1986; Haubensack, 1981). The fine-grained black levels are

51 composed of detrital quartz, plagioclase and biotite. Plagioclase and biotite are locally replaced
52 by calcite and illite + chlorite assemblage respectively (Haubensack, 1981). The green colored
53 intermediate levels are rich in illite (or phengite) and chlorite which replace detrital biotite and
54 locally feldspar. The sandstone is mainly composed of quartz grains cemented by calcite, illite
55 and chlorite. The conglomeratic sandstones at the base of the FA sedimentary series lie directly
56 on the granitoid basement. Their mineralogical composition is dominated by a microcrystalline
57 illitic material filling the porosity and replacing feldspars. When disseminated between quartz
58 crystals, the illitic matrix may contain calcite, anhydrite or gypsum. The sandstones at the very
59 base of the series, are known to be red colored due to the precipitation of hematite in the
60 cleavages of altered biotites and to the staining of detrital quartz grain surfaces. This is not the
61 case in the eight studied drills crosscutting the unconformity we studied here: no trace of red
62 coloration has been observed probably because detrital ferromagnesian minerals are lacking or
63 perhaps, because of a secondary discoloration.

64 **3. Sampling and analytical methods**

65 **3.1 Sampling**

66 The eight drill cores studied here are located in the Kiéné region (250 km^2), the central part of
67 the Franceville basin, close to the Mikouloungou U-ore deposit and the Kaya-Kaya fault (Fig.
68 2a). Petrographic investigations were performed on 38 samples collected along the eight drill
69 cores (KA 13, GR1, GR5, GR23, GR31, GR20 GR43 and KA6) down to variable depth (5 to 36
70 m) below the unconformity between sandstones and granitic basement (Fig. 2b). From the
71 deepest levels to the sediment interface, the granitoids exhibit three dominant “facies” which
72 correspond to an increasing alteration degree: (i) the least altered one, observed at depth, are gray

73 TTG or pink-to-red syenitic-to-granitic rocks; (ii) the altered granitoids in which the initial
74 petrographical texture is preserved; (iii) the intensely altered granitoids which are green colored
75 close to the sandstone-basement unconformity for all the studied drill-cores. The granitoids are
76 largely altered and red colored near the sandstone contact in the GR20 and GR31 drill cores (Fig.
77 2b).

78 **3.2 Analytical methods**

79 The petrographical observations of the granitoids were performed using optical and scanning
80 electron microscopes (OM, SEM). Polished thin sections were carbon coated before examination
81 using the backscattered electron mode imaging (Jeol JSM 5600LV). X-ray spectra were collected
82 with an energy dispersive device according to following analytical conditions: 15 kV accelerating
83 voltage, 1 nA probe current and a 16.5 mm focalization distance. Micro-chemical analyses were
84 obtained using a CAMECA SX50 electron microprobe (CAMPARIS analytical center, University
85 Pierre and Marie Curie, Paris VI) equipped with wavelength dispersive spectrometers (15 kV
86 accelerating voltage, 1 nA probe current, 1 μ m beam spot diameter). Bulk rock analyses were
87 carried out at the SARM-CRPG (Nancy, France; Table 1). The samples were fused with LiBO₂,
88 dissolved with HNO₃, analyzed using ICP-EAS and ICP-MS for major and trace elements
89 respectively. The calibration is based on international standards. The mineralogical composition
90 of each sample has been determined using X-ray diffraction of randomly oriented powders
91 (Bruker D8 ADVANCE A25 diffractometer, CuK α). The accelerating voltage and probe current
92 were of 40KV and 40 mA, respectively. Clay mineral identification was detailed using oriented <
93 2 μ m preparations scanned in the air dried and ethylene glycol saturation states in the 8 to 30° 20
94 CuK α angular range. The C and O isotope compositions of calcitic veins were measured in the
95 stable isotope laboratory of the Géosciences department (Rennes, University of Rennes 1).

96 Calcite was reacted with anhydrous H₃PO₄ at 50°C and the isotopic compositions measured on a
97 triple collector VG Optima mass spectrometer.

98 The monazite crystals observed in two samples (KA6 437.85 and GR1 631) near the
99 unconformity level were used to constrain the ages of plutonic rock emplacement and their
100 subsequent alterations. These crystals were examined using SEM, mostly in backscattered
101 electron mode, and analyzed using a CAMECA SX50 electron microprobe (CAMPARIS center,
102 University Pierre and Marie Curie, Paris VI). U-Th-Pb isotopic data were obtained by laser
103 ablation inductively coupled plasma spectrometry (LA-ICPMS) at the Volcanology Laboratory of
104 Clermont-Ferrand University. The analyses involved the ablation of minerals using a Resonetics
105 Resolution M-50 powered by an ultra-short-pulse (<4ns) ATL Atlex Excimer laser system
106 operating at a wavelength of 193 nm (Muller et al., 2009). A 7 µm laser spot diameter and
107 repetition rate of 1 Hz with energy of 8 mJ producing a fluence of 15 J/cm² was used for zircon
108 dating. The ablated material was carried into helium flux and then mixed with nitrogen and argon
109 before injection into the plasma source of an Agilent 7500 cs ICP-MS equipped with a dual
110 pumping system to enhance the sensitivity. The alignment of the instrument and mass calibration
111 were performed before each analytical session using the NIST SRM 612 reference glass, by
112 inspecting the signal of ²³⁸U and by minimising the ThO⁺/Th⁺ ratio (< 1%). The mean sensitivity
113 for ²³⁸U using a spot size of 44 µm is about 25,000 cps/ppm. The analytical method for isotope
114 dating of zircon with laser ablation ICPMS is similar to that developed for monazite and reported
115 by Paquette and Tiepolo (2007). The signals of ²⁰⁴(Pb+Hg), ²⁰⁶Pb, ²⁰⁷Pb, ²⁰⁸Pb, ²³²Th and ²³⁸U
116 masses are acquired. The occurrence of common Pb in the sample can be monitored by the
117 evolution of the ²⁰⁴(Pb+Hg) signal intensity, but no common Pb correction was applied owing to
118 the large isobaric interference from Hg. The ²³⁵U signal is calculated from ²³⁸U on the basis of the

ratio $^{238}\text{U}/^{235}\text{U}$ = 137.88. The analyse procedure is based on 30 seconds of background integration with laser off followed by 1 minute integration with the laser firing and a 30 seconds delay to wash out the previous sample and prepare the next analysis. Data are corrected for U-Pb fractionation occurring during laser sampling and for instrumental mass discrimination (mass bias) by standard bracketing with repeated measurements of the Moacyr monazite standard (Gasquet et al., 2010). Repeated analyses of Manangoutry monazite standard (Paquette and Tiepolo, 2007), treated as unknown, independently control the reproducibility and accuracy of the corrections. Data reduction was carried out with the software package GLITTER[®] from Macquarie Research Ltd (Achterbergh et al., 2001; Jackson et al., 2004). For each analysis, the time resolved signal of single isotopes and isotope ratios was monitored and carefully inspected to check the presence of perturbations related to inclusions, fractures, mixing of different age domains or common Pb. Calculated ratios were exported and Concordia $^{206}\text{Pb}/^{238}\text{U}$ vs $^{208}\text{Pb}/^{232}\text{Th}$ ages and diagrams were generated using the Isoplot/Ex v. 3.23 software package (Ludwig, 2001).The concentrations in U-Th-Pb were calibrated relative to the certified contents of Moacyr monazite standard (Seydoux-Guillaume et al., 2002).

134 4. Results

135 4.1. The least-altered granitoids

136 The least altered gray or pink-to-red granitoids are observed in the deepest parts of the
137 different drill cores far from the unconformity (Fig. 2b). The primary minerals are quartz,
138 plagioclase (An₀ –An₂₀), biotite, alkali feldspar and locally amphibole. Zircon, apatite,
139 uranothorite and monazite are the common accessory mineral phases. The gray granitoids present
140 sometimes a gneissic structure.

141 The magmatic rocks range from diorite to granite. The whole rock major element compositions
 142 of the less altered rocks reflect the variety of these rock types (Table 1): i.e. SiO₂ (52.1 - 74.5
 143 wt%), FeO_T (0.3 - 9.5 wt%), MgO (0.16 - 6.7 wt%). In order to determine their magmatic type,
 144 the chemical composition of these rocks has been plotted in the Q-P chemical-mineralogical
 145 diagram of Debon and Le fort (1983) (Fig.3). Because even the best preserved samples from the
 146 eight drill cores exhibit petrographic features of a hydrothermal alteration event the rock samples
 147 were selected according to their low ignition loss value: 2.5 Wt%. The grey TTGs range from
 148 quartz-diorite (dq) to tonalite (to) composition, while the pink and red rocks correspond to
 149 granodiorite (gd) and adamellite (ad) (Table 1; Fig. 3). The chondrite-normalized REE patterns
 150 show that tonalities present the typical highly fractionated pattern: high LREE content, low
 151 HREE content, no significant Eu anomaly. These properties are typical of the Archean TTG
 152 (Martin, 1986). On the other hand, the granodiorite and adamellite have lower REE contents with
 153 a positive Eu anomaly; such REE patterns have already been interpreted in Archean rocks as
 154 resulting from the fractionation by accessory phases such as allanite and zircon (Martin,
 155 1987)(Fig. 4). Finally the higher REE content of the diorite is similar to that of the late Archean
 156 sanukitoids (Martin et al., 2010; Stern, 1989). In other words, all the less altered rock samples
 157 display the features typical of late Archean magmatic associations.

158 **4.2. The altered granitoids**

159 ***4.2.1. Samples located far from the unconformity***

160 All the Kiéné granitoid samples located far from the unconformity exhibit the presence of
 161 chlorite. A pervasive chloritization process has severely affected the primary ferromagnesian
 162 minerals, i.e. total replacement of biotite and amphibole. Chlorite is associated to epidote, titanite

163 and allanite (Fig. 5a). According to Lowell and Guilbert, (1970) and Titley et al. (1986), this
 164 paragenesis is typical of a propylitic alteration. Concomitantly, the plagioclases are partially
 165 replaced by small sized micas (sericite) forming a microcrystalline matrix in which calcite, pyrite
 166 and chalcocryrite crystals are locally disseminated. Some fractures crosscut the propylitized
 167 rocks. They are filled by a zoned deposit: chlorite along the walls and calcite sealing the central
 168 part (fig. 5b)

169

170 ***4.2.2. Samples close to the unconformity***

171 The Kiéné granitoids are affected by an intense illitization in the vicinity of unconformity
 172 giving them a green color. This alteration is mainly invasive and extends down to 4-5 m depth.
 173 Plagioclase, K-feldspar and previously chloritized biotite are totally or partially replaced by illite
 174 (Fig.6a and b). The feldspars are corroded by a microcrystalline matrix (5-20 μm) while the
 175 chloritized biotite are replaced by larger illite crystals (10-50 μm). The quartz bodies, themselves,
 176 exhibit corrosion features and are locally crosscut by illite veinlets. The illitization intensity
 177 decreases with depth becoming nearly undetectable between 5 and 7 m down from the
 178 unconformity. Here, only illite veinlets are still observable. Close to the unconformity, the GR20,
 179 GR23 and GR31 granitoid samples become red colored. The chloritized biotites are replaced by
 180 an illite + hematite assemblage (Fig. 6b). The rocks are crosscut by calcite \pm anhydrite veins (Fig.
 181 6c). Some monazites have been locally observed disseminated through the illitic matrix.

182

183 ***4.2.3. Alteration features of FA sandstones***

184 The FA sandstones above the unconformity exhibit detrital quartz and K-feldspar crystals
 185 embedded in an illitic micro-crystalline matrix while the detrital grains, whatever their
 186 composition, are invaded along their inter-granular joints. Samples GR23 629 and GR20 818 are
 187 cemented by anhydrite and/or calcite deposits (Fig. 6d).

188

189 **4.3. Geochemical data of bulk rocks**

190 Because of the predominance of hydrolyzed and carbonated secondary phases in the secondary
 191 minerals, the loss on ignition (L.O.I) has been chosen here as an indicator of the alteration
 192 degree. In most samples, L.O.I. is significantly greater than that of the corresponding unaltered
 193 rocks. Indeed, the measured values range from 0.76 wt% in the freshest granitoids to 4.5 wt% for
 194 the most altered. However, the average L.O.I. calculated from a compilation of 60 TTG samples,
 195 is much lower: 0.25 wt% (Huang et al., 2013). Consequently, the absolute value of L.O.I. cannot
 196 be directly used as a reliable marker because of two reasons: (i) for a given rock type, it depends
 197 on the quantity of secondary minerals produced by alteration processes; (ii) it varies according to
 198 rock types. For instance, diorite L.O.I. typically averages to 1.55 wt% (Debon and Le Fort, 1983),
 199 tonalite for 0.32 and granodiorite for 0.12 (Huang et al., 2013). The tonalite value will be used
 200 here as the reference in the calculation of relative L.O.I. variations $\Delta LOI = (LOI_{sample} -$
 201 $LOI_{ref})/(LOI_{most\ altered\ sample} - LOI_{ref})$. According to this definition, the ΔLOI calculated for each
 202 basement sample shows a regular increase toward the unconformity (Fig. 9). The most altered
 203 levels are found in the illitic zone in agreement with petrographic observations. In order to
 204 address the problem of element mobility, it appears suitable to normalize all chemical element
 205 values to that one remaining immobile during the alteration processes. As already proposed by

several authors (Nesbitt, 1979; Ohmoto, 1996; Rye and Holland, 1998; White et al., 2001), Ti or Zr are classically considered as reference immobile elements. Here, Ti has been chosen because of its higher content. Then, each element content in the altered samples is corrected by the $\text{TiO}_2^{\text{reference}}/\text{TiO}_2^{\text{sample}}$ ratio. Propylitic and illitic processes being acceptably discriminated by the increasing loss on ignition (Fig. 7), the ΔLOI parameter has been used to study the variations of the major and some minor element amounts as a function of alteration intensity (Figs. 8 and 9). These variations between altered and reference samples (defined by the lowest ΔLOI) are calculated as follows: $\Delta\text{SiO}_2^{\text{sample}} = (\text{SiO}_2^{\text{sample}} \times \text{TiO}_2^{\text{reference}}/\text{TiO}_2^{\text{sample}}) - \text{SiO}_2^{\text{reference}}$ (wt%). Because the piece of rocks sampled in the drill cores cannot be at the size of a representative sample, the experimental error is not calculable. This is why we adapted the variation scales to their abundance in the specimens: 0 to 50 for SiO_2 and Al_2O_3 , -7 to 2 for all the other components. Reported in the same scale, ΔSiO_2 and $\Delta\text{Al}_2\text{O}_3$ show contrasted distribution with ΔLOI : the first one is systematically negative while the second remains roughly constant. Silica loss and aluminium conservation are commonly reported in water rock interactions due to their large difference of solubility. The weight percent variations are more limited for Fe_2O_3 , MgO and CaO . If they are not significant for the first and second ones, it seems that the losses of the calcium are more important in the illitic alteration zone. The chemical differences between propylitized and illitized samples are clearly evidenced by the alkaline element behaviour. All exhibit increasing losses of Na_2O with ΔLOI but they more important for the second ones. The K_2O amount remains roughly constant in the propylitized zone while it significantly increases in the illitic one. The variations for trace elements are expressed in ppm (Fig. 9). The illitized samples are enriched in rubidium and cesium because of their potassium similar chemical affinities for micas. Strontium is depleted in all the samples, the losses being more important in

229 the illitized ones. Cerium and lanthanum amounts are highly variable in the propylitized samples
230 while they are systematically depleted in the illitized ones (Figs. 9 and 10). The variations of
231 uranium are erratic but thorium seems to be systematically depleted. In spite of the uncertainties
232 due to the limited size of the samples, it is possible to distinguish the geochemical characteristics
233 of the two alteration types. Indeed, the propylitic alteration is almost chemically conservative: the
234 losses of SiO_2 and Na_2O are limited. This is not the case for illitization which is depleted in all
235 the components except aluminium (conserved) and potassium (enriched). The behaviour of trace
236 elements outlines this difference.

237 **4.4. Crystalllo-chemistry of secondary phases**

238 Chlorite and illite-phengite are present in all the studied samples. It is to be noticed that no di-
239 or trioctahedral expandable mixed-layer minerals have been detected in the studied samples (Fig.
240 11a).

241 **4.4.1. Chlorite**

242 XRD patterns of randomly oriented powders show that chlorites are of the IIb polytype. The
243 (001)/(002) peak intensity ratio decreases from depth to top (0.60-0.50 to 0.20) indicating that the
244 relative proportion of Fe and Mg ions changes from the deep propylitic zone to the upper illitic
245 level (Fig. 11b). This is coherent with the micro-chemical analyses of individual chlorite crystals.
246 Most of the half-formula units calculated on a 14 oxygen basis, plot inside the brunsvigite
247 composition field defined by Foster (1960). This is the case for all the chlorites in the propylitic
248 zone (Table 2, Table 3, Fig. 12b). The $\text{Fe}/(\text{Fe}+\text{Mg})$ ratio varies from 0.3-0.5 (propylitic zone) to
249 0.6 – 0.7 (illitic level).

250 **4.4.2. Illite-phengite**

251 The XRD patterns of randomly oriented powders indicate that the illite-phengite minerals are
 252 composed of a mixture of 2M₁ and 1M polytypes. They are small sized crystals when replacing
 253 the feldspars or infilling the quartz microcracks (5-20µm) but become larger when replacing
 254 chlorites (10-50µm). Their half-formula units calculated from microprobe analyses using a 11
 255 oxygen basis, are coherent with that of dioctahedral micaceous minerals (Tables 4, 5). Two
 256 populations are clearly separated in the MR³⁺, 2R³⁺, 3R²⁺ diagram proposed by Velde (1985). The
 257 phengitic crystals are found in the altered chlorites as shown by the mixing line while the illitic
 258 ones are found in the altered feldspars (Fig. 12a). Both exhibit a quite similar range of
 259 Fe/(Fe+Mg) ratio: 0.46-0.61 and to 0.52-0.76 for phengite and illite respectively. However,
 260 phengites are always K-richer than illite: 0.84-0.95 and 0.73-0.84 respectively.

261 ***4.4.3. Epidote-allanite***

262 Epidotes are of the pistachite type (Table 6). They form everywhere in the rock, partly
 263 replacing primary feldspars or chloritized biotites or precipitating into veinlets. Their Fe/(Fe+Al)
 264 ratio varies from 0.30 to 0.42. Allanite crystals, on the contrary, form exclusively in chloritized
 265 biotites. They present a rather constant Fe/(Fe+Al) ratio (0.3-0.32). Their main chemical
 266 characteristic is the very high Nd, Ce and La contents: 0.16-0.07, 0.38-0.36, 0.25-
 267 0.17%respectively.

268 ***4.4.4. Monazite***

269 Monazite crystals have been observed in two samples: KA6 437.85 (0.85 m from the
 270 unconformity) and GR1 631 (1 m from unconformity). The first one is a strongly illitized rock
 271 containing Fe-rich chlorites. Euhedral elongated millimeter size crystals of monazite are scattered
 272 in the illitic matrix. They seem to be perfectly unaltered and do not exhibit any chemical zoning

273 in spite of light grey intensity variations observed in the BSE imaging contrast (Table 7). The
 274 GR1 631 sample is less illitized since only feldspars are altered. Most of the micro-cracks are
 275 filled by calcite, and locally by quartz and pyrite. Here, the monazite crystals are anhedral, often
 276 grouped in aggregates and intimately associated with sulfide and illite. Compared to the euhedral
 277 crystals of the KA6 437.85 sample, monazite crystals of the GR1 631 one exhibit higher U, La
 278 and Ce and lower Th, Ca, Nd, Sm contents. The Th/U ratios are very low (Tables 8.9). They are
 279 characterized by lower Th content (Th<12000 ppm) compared to that of the unaltered monazites
 280 described by Mathieu et al. (2001) in the FA Sandstone (average Th = 40000 ppm for 94
 281 analyses).

282 **4.4.5. Carbonates**

283 Calcite is observed in many samples from depth to the upper levels in the FA sandstone. Far
 284 from the unconformity in the propylitic zone, it appears as xenomorphic crystals located in
 285 altered plagioclase and in veinlets where it is associated to chlorite. It is observed as euhedral
 286 crystals filling the fissures near the unconformity where it is locally associated to anhydrite. In
 287 some of the FA sandstone samples, it constitutes the inter-granular microcrystalline cement.
 288 Regardless of their habit, the calcite crystals do not show significant chemical composition
 289 differences.

290 **4.5. Geochronological data**

291 The isotopic dating using laser-ICPMS microanalyses were performed on monazite crystals
 292 sampled near the FA sandstone-granitoid unconformity in the KA6 437.85 and GR1631 (Tables 8
 293 and 9). The first one is Th-rich (11614-2909 ppm). Plotted in the $^{206}\text{Pb}/^{238}\text{U}$ versus $^{207}\text{Pb}/^{235}\text{U}$
 294 diagram (Fig. 13), the U-Pb data of the KA6 437.85 monazite give two groups of discordia ages:

295 from 2998 ± 25 Ma (MSWD = 0.72) to 2922 ± 24 Ma (MSWD = 1.4) and 2621 ± 30 Ma (MSWD =
 296 1.5). The GR1 631 monazite being common Pb-rich, the dating is obtained using the $^{207}\text{Pb}/^{206}\text{Pb}$
 297 versus $^{206}\text{Pb}/^{238}\text{U}$. The Tera-Wasserburg diagram (Fig. 14) gives an age of 1870 ± 26 Ma (MSWD
 298 = 1.04).

299

300 **4.6. C and O isotope compositions of calcite**

301 The calcite isotopic analyses were performed on the propylitized and illitized granitoids far
 302 from and closed to the unconformity respectively. The $\delta^{13}\text{C}$ values obtained varies from -5 to -
 303 $14\text{\textperthousand}$ and the $\delta^{18}\text{O}$ ones from 10.2 and $17.7\text{\textperthousand}$, most of them being close to $10.5 - 11\text{\textperthousand}$ (Tab. 10).
 304 The C and O isotope compositions are not inter-correlated, nor with depth, intensity of
 305 carbonation, nature of alteration (propylitization, illitization), or element mobility.

306 The large range of $\delta^{13}\text{C}$ values suggest that carbon comes from two different sources: one
 307 having a $\delta^{13}\text{C} > -5\text{\textperthousand}$, which might be surface-derived continental carbon including atmospheric
 308 CO_2 , and another one having a $\delta^{13}\text{C} < -14\text{\textperthousand}$, which could possibly be a signature of the evolved
 309 organic matter similar to that identified in the sediments of the Franceville Basin (Albani et al.,
 310 2010; Weber and Gauthier-Lafaye, 2013). The $\delta^{18}\text{O}$ values centered around $10.5 - 11\text{\textperthousand}$ point to
 311 formation at low temperature hydrothermal conditions ($150-300^\circ\text{C}$), which is consistent with the
 312 common mineralogical association of calcite + chlorite, where the fluids reached isotopic
 313 equilibrium with the granitic basement. On the other hand, the KA6462 sample has a much
 314 higher $\delta^{18}\text{O}$ value, which probably relates to calcite formation at lower temperatures than for the
 315 others, regardless of the nature of the fluid involved in calcite crystallization.

316 As a whole, the C and O isotope compositions are consistent with the presence of a diagenetic
 317 fluid that would have circulated along or close to the unconformity, imposing low temperature
 318 hydrothermal conditions to secondary alteration processes as it is the case for the Athabasca basin
 319 (Richard et al., 2013). Part of the carbon was taken from the organic matter which is particularly
 320 abundant in the FB Francevillian sediments. A similar case is given by the Athabasca basin
 321 where metamorphic fluids have interacted with graphite bearing metasediments of the basement.
 322 These fluids have been able to precipitate calcite with such isotopic signatures, at greenschists
 323 conditions, in equilibrium with chlorite.

324 **5. Discussion**

325 **5.1. Propylitic alteration**

326 Sère (1996) interpreted the presence of chlorite, albite, quartz and calcite in veins crosscutting
 327 the Chaillu massif as witnessing a metamorphic episode of the greenschist facies type. The
 328 petrographic observation performed on the eight drill cores show that all the biotite crystals have
 329 been chloritized regardless of the parent rock type: granitoids or gneiss. This implies that the
 330 chloritization took place after deformation. Consequently, it cannot be related to a metamorphic
 331 event but rather to a propylitic alteration which preserves the texture of rocks. Indeed, the
 332 chlorite-sericite-epidote/calcite assemblage is commonly described in propylitized granitoids
 333 (Lowell and Guilbert, 1970; Titley et al., 1986).

334 The $\Delta\text{Fe}_2\text{O}_3/\text{TiO}_2$, $\Delta\text{MgO}/\text{TiO}_2$, $\Delta\text{CaO}/\text{TiO}_2$, and $\Delta\text{K}_2\text{O}/\text{TiO}_2$ ratios do not vary with ΔLOI in the
 335 propylitic zone (Fig 10). Some samples plot far from general trend due to the local invasion by
 336 secondary minerals such as calcite (high CaO/TiO_2 ratio-GR23 631) in fracture and plagioclase.
 337 The $\Delta\text{SiO}_2/\text{TiO}_2$ and $\Delta\text{Na}_2\text{O}/\text{TiO}_2$ ratios decrease slightly while $\Delta\text{Al}_2\text{O}_3/\text{TiO}_2$ remains roughly

338 constant. This means that the propylitized rocks do not have experienced significant exchanges of
 339 chemical component with the external reservoir. It is a nearly isochemical set of mineral reactions
 340 in which the potassium released by biotite during chloritization is consumed by the crystallization
 341 of sericite. This is typical of propylitic alteration in which the water/rock ratio is limited (Berger
 342 and Velde, 1992). The temperature conditions can be roughly estimated using mineral indicators.
 343 The allanite is known to be found at rather high temperature: 400 °C (Berger and Velde, 1992;
 344 Smith and Barreiro, 1990; Wing et al., 2003) while the chlorite-epidote-paragenesis is formed in
 345 the range 350 to 200 °C (Norman et al., 1991). These conditions are compatible with that
 346 prevailing during the cooling stage following the intrusion of plutonic rocks.

347 **5.2 Illitic alteration**

348 Petrographic observations suggest that the propylitic alteration is overprinted by an illitic one
 349 in the upper part of the basement within 4-5 m below the unconformity. It is typically
 350 characterized by a massive replacement of all the primary and secondary minerals except the
 351 sericite zones in feldspars which seem to have been preserved. This could explain the co-
 352 existence of the 2M₁ and 1M polytypes of the white micas fraction. The degree of replacement
 353 decreases with depth down to 7 m where illite is observed only in veins. Epidote and allanite
 354 have totally disappeared while chlorite seems to remains up to the unconformity. However, its
 355 composition changes becoming iron-richer composition. This indicates that it has recrystallized
 356 in a more stable version considering the local chemical condition imposed by the fluid
 357 responsible of the illitic alteration. As shown by the strong decrease of the ΔCaO and ΔNa₂O
 358 ratios on one hand and the increase of the ΔK₂O ones on the other hand, it appears that the illitic
 359 alteration induces more important chemical changes of the rocks than the propylitic one did (Fig.
 360 8). It is obvious that it operates in an open system in which the fluids have flowed. The mineral

361 similarities between illite in the most altered basement samples and the upper sandstones militate
362 for extensive chemical exchanges driven by the diagenetic fluids along the unconformity. The
363 very low thorium content of the small euhedral monazite crystals indicates that they have
364 crystallized at low temperature (Overstreet, 1960) and are probably synchronous with the illitic
365 alteration.

366 **5.3. Could a paleosol have been present along the unconformity?**

367 Based on the study of fifty pre-Devonian rock units that have been described as paleosols, Rye
368 and Holland (1998) proposed that five criteria must be respected to evidence the weathering
369 effects: (*i*) the paleosol is developed on a homogeneous parent rock and has been preserved in
370 place; (*ii*) textural; (*iii*) mineralogical; (*iv*) chemical; (*v*) soft sediments features. A geological
371 formation that meets all these criteria is classified as definite paleosol; when all criteria are met
372 but one it is likely a paleosol; all but two is a possible paleosol; not more than three criteria is
373 unlikely a paleosol.

374 Considering the eight drill cores studied here, no petrographic features typical of a weathering
375 process have been observed, even in the reddish samples from the GR31 or the GR20 drill cores.
376 None of them contain any evidence of typical weathering processes such as primary phase
377 recrystallization inside microsystems, clay translocation deposits (cutans) or increasing porosity
378 toward the surface (Velde and Meunier, 2008). On the contrary, the rocks, irrespective of their
379 petrographic properties, are all invaded by a single clay mineral phase: illite. If any physical
380 traces of a weathering event have been preserved after the sediment deposition, they have been
381 totally erased by the diagenetic alteration processes.

382 As it is the case for any water/rock interactions induced by pure water or diluted solution
383 invasion, the most soluble components are leached out from the altered rock (Ca, Na, Mg) while
384 the less soluble (Al, Ti) ones are concentrated and K is enriched (Fig. 8). These chemical
385 characteristics do not meet the criteria proposed by Rye and Holland (1998). Consequently, the
386 probability for a paleosol to have been formed on the unconformity surface before being buried
387 under the sediments of the Franceville basin is very weak. The superimposition of an illitic
388 alteration upon a previous propylitic one is the most probable scenario here. It is supported by the
389 distinct chemical trends evidenced by plotting the bulk rock compositions in the Al_2O_3 - CaO ,
390 Na_2O , K_2O - FeO , MgO system (Fig. 15). Two trends are clearly separated: (i) a shift toward the
391 epidote-chlorite assemblage typical of the propylitic alteration or magmatic differentiation; (ii) a
392 shift toward the illite pole. The two different chemical pathways are coherent with the
393 progressive upward variation of Rb, Cs and Sr amounts which are increasing and decreasing
394 respectively (Fig. 9). The same contrasted chemical behavior is also observed for the REE
395 distribution: the amounts of the light ones (LREE) do not vary during the propylitic alteration
396 while they are leached out during the illitic event (Fig. 9 and 10). This is also coherent with the
397 disappearance of the allanite crystals which could be related to the percolation of oxidizing
398 diagenetic fluids invading the basement from the overlying sedimentary basin through the
399 unconformity (Cuney and Mathieu, 2000).

400 The negative $\delta^{13}\text{C}$ values of calcite crystals in veins indicate that the diagenetic fluids involved
401 in the illitization process were mixed with organic compounds deriving from oil maturation in the
402 FB sediments (Gauthier-Lafaye and Weber, 1989; Weber and Gauthier-Lafaye, 2013).

403 **5.4. Timing of alteration events.**

404 The isotopic U-Pb data gathers into three major dating groups. The oldest one, from 2998 ± 25
 405 Ma to 2922 ± 24 Ma is consistent with the age of plutonic intrusions forming the basement. The
 406 2621 ± 30 Ma intermediate group might correspond to the hydrothermal propylitic event related
 407 to the intrusion of the neoarchean plutonic bodies. It is to be noticed that the dating obtained here
 408 from monazite crystals is coherent with that measured in altered biotites using the K-Ar method:
 409 2696 ± 60 Ma (Bonhomme et al., 1978). The youngest group, i.e. 1870 ± 26 Ma, has been
 410 measured on newly formed monazites from the illitized zone. Their extremely low Th contents
 411 reflect a crystallization process under low temperature conditions. It is consistent with the
 412 diagenetic event of the Franceville basin (Bonhomme et al., 1982).

413 **6. Conclusion**

414 The mineralogical and geochemical studies of the basement of the Franceville Basin along a
 415 nearly E-W profile show that the basement is composed of different plutonic rocks. Dating
 416 obtained from 8 drill holes give Archean ages (3.0 – 2.9 Ga) similar to the ones obtained on rocks
 417 outcropping in the Chaillu Massif. No metasedimentary formations have been intersected. Most
 418 of these rocks present evidences of a propylitic alteration which postdate any ductile deformation
 419 and which may be associated to the intrusion of some Neoarchean plutonic rocks at about 2.6 to
 420 2.7 Ga (Thiéblemont et al., 2009). The mineral reactions produced a Mg chlorite + epidote +
 421 allanite + titanite paragenesis typical of nearly close systems: no significant mobility of the major
 422 elements suggesting weak Water/Rocks ratios. Then, a massive illitic alteration associated with
 423 hematization, has transformed the previously propylitized rocks over a thickness of 2 to 5 m
 424 below the unconformity in the Franceville basin. It has been triggered by the percolation of
 425 oxidizing diagenetic fluids from the FA conglomeratic-sandstone formation at the base of the
 426 sedimentary basin through the unconformity. Similar fluid invasions have been described in other

427 basins: Southern Norway (Munz et al., 1995; Oliver et al., 2006), Spain (Bouch et al., 2006),
 428 France, Northwestern Massif Central (Munoz et al., 1999), Athabasca, Canada (Richard et al.,
 429 2013) and Kombolgie, Australia (Derome et al., 2003). Most of the major and light Rare Earth
 430 elements have been heavily depleted. This is particularly the case for Ca, Na and Mg while Al
 431 amounts are roughly preserved. No paleosol chemical or petrographical traces have been detected
 432 here. The calcite $\delta^{13}\text{C}$ values confirm the diagenetic origin for the fluids which have percolated
 433 into the basement. They were also responsible of the uranium transfer and deposition in the
 434 vicinity of the organic-rich sediments of the FB formation which gave the natural nuclear reactors
 435 (Gauthier-Lafaye and Weber, 2003; Mathieu et al., 2000).

436

437 AKNOWLEDGMENT

438 We thank the Gabonese Government, the Sylvia Bongo Foundation, Région Poitou-Charentes,
 439 FEDER program, CNRS-INSU and University of Poitiers for their financial supports.
 440 We also thank the « Direction Générale des Mines et de la Géologie du Gabon » (DGMG) for
 441 its technical support.

442

443 REFERENCES

- 444 Achterbergh, E., Ryan, C.G., Jackson, S.E., and Griffin, W.L., 2001, Data reduction software for
 445 LA-ICP-MS: In: Laser ablation-ICPMS in the earth science. P. Sylvester ed.
 446 Mineralogical Association of Canada, v. 29, .
- 447 Albani, A.E., Bengtson, S., Canfield, D.E., Bekker, A., Macchiarelli, R., Mazurier, A.,
 448 Hammarlund, E.U., Boulvais, P., Dupuy, J.-J., Fontaine, C., Fürsich, F.T., Gauthier-
 449 Lafaye, F., Janvier, P., Javaux, E., Ossa, F.O., Pierson-Wickmann, A.-C., Riboulleau, A.,
 450 Sardini, P., Vachard, D., Whitehouse, M., and Meunier, A., 2010, Large colonial

- 451 organisms with coordinated growth in oxygenated environments 2.1[thinsp]Gyr ago:
 452 *Nature*, v. 466, p. 100-104.
- 453 Berger, G., and Velde, B., 1992, Chemical parameters controlling the propylitic and argillic
 454 alteration process: Stuttgart, ALLEMAGNE, Schweizerbart.
- 455 Bonhomme, M., Leclerc, J., and Weber, F., 1978, Etudes radiochronologique complémentaire de
 456 la série du Francevillian et de son environnement: In: IAEA, editors. Les réacteurs de
 457 fission naturels, Vienne,, p. 19-23.
- 458 Bonhomme, M.G., Gauthier-Lafaye, F., and Weber, F., 1982, An example of lower proterozoic
 459 sediments: The Francevillian in Gabon: *Precambrian Research*, v. 18, p. 87-102.
- 460 Bouch, J., Naden, J., Shepherd, T., McKervey, J., Young, B., Benham, A., and Sloane, H., 2006,
 461 Direct evidence of fluid mixing in the formation of stratabound Pb–Zn–Ba–F
 462 mineralisation in the Alston Block, North Pennine Orefield (England): *Mineralium*
 463 *Deposita*, v. 41, p. 821-835.
- 464 Bouton, P., Thiéblemont, D., Gouin, J., Cocherie, A., Guerrot, C., Tegyey, M., Préat, A., Simo
 465 Ndounze, S., and Moussavou, M., 2009, Notice explicative de la carte géologique de la
 466 République du Gabon à 1/200 000, feuille Franceville-Boumango: . Edition DGMG-
 467 Ministère des Mines, du Pétrole, des Hydrocarbures, Libreville,, p. 79 p.
- 468 Caen-Vachette, M., Vialette, Y., Bassot, J.P., and Vidal, P., 1988, Apport de la géochronologie
 469 isotopique à la connaissance de la géologie gabonaise: *Chronique de Recherche Minière*,
 470 v. 491, p. 35-54.
- 471 .
- 472 Card, K.D., 1978, Metamorphism of the Middle Precambrian (Aphebian) rocks of the eastern
 473 southern Province: *Metamorphism in the Canadian Shield*; by Fraser, J A (ed.); Heywood,
 474 W W (ed.); Geological Survey of Canada,, v. 78-10, p. 269-282.
- 475 Chevallier, L., Makanga, J.F., and Thomas, R.J., 2002, Notice explicative de la Carte géologique
 476 de la République Gabonaise à 1/ 1 000 000: Editions DGMG Gabon, p. 195.
- 477 Cuney, M., and Mathieu, R., 2000, Extreme light rare earth element mobilization by diagenetic
 478 fluids in the geological environment of the Oklo natural reactor zones, Franceville basin,
 479 Gabon: *Geology*, v. 28, p. 743-746.
- 480 Debon, F., and Le Fort, P., 1983, A chemical–mineralogical classification of common plutonic
 481 rocks and associations: *Earth and Environmental Science Transactions of the Royal*
 482 *Society of Edinburgh*, v. 73, p. 135-149.
- 483 Derome, D., Cuney, M., Cathelineau, M., Fabre, C., Dubessy, J., Bruneton, P., and Hubert, A.,
 484 2003, A detailed fluid inclusion study in silicified breccias from the Kombolgie
 485 sandstones (Northern Territory, Australia): inferences for the genesis of middle-

- 486 Proterozoic unconformity-type uranium deposits: JOURNAL OF GEOCHEMICAL
 487 EXPLORATION, v. 80, p. 259-275.
- 488 Gasquet, D., Bertrand, J.-M., Paquette, J.-L., Lehmann, J., Ratzov, G., De Ascenção Guedes, R.,
 489 Tiepolo, M., Boullier, A.-M., Scaillet, S., and Nomade, S., 2010, Miocene to Messinian
 490 deformation and hydrothermal activity in a pre-Alpine basement massif of the French
 491 western Alps: new U-Th-Pb and argon ages from the Lauzière massif: Bulletin de la
 492 Societe Geologique de France, v. 181, p. 227-241.
- 493 Gauthier-Lafaye, F., 1986, Les gisements d'uranium du Gabon et les reacteurs d'Oklo. Modèle
 494 métallogénique de gîtes à fortes teneurs du protérozoïque inférieur: Thèse de Doctorat
 495 d'Etat, Université de Strasbourg, p. 206.
- 496 Gauthier-Lafaye, F., Holliger, P., and Blanc, P.L., 1996, Natural fission reactors in the
 497 Franceville basin, Gabon: A review of the conditions and results of a “critical event” in a
 498 geologic system: *Geochimica et Cosmochimica Acta*, v. 60, p. 4831-4852.
- 499 Gauthier-Lafaye, F., and Weber, F., 1989, The Francevillian (Lower Proterozoic) uranium ore
 500 deposits of Gabon: *Economic Geology*, v. 84, p. 2267-2285.
- 501 Gauthier-Lafaye, F., and Weber, F., 2003, Natural nuclear fission reactors: time constraints for
 502 occurrence, and their relation to uranium and manganese deposits and to the evolution of
 503 the atmosphere: *Precambrian Research*, v. 120, p. 81-100.
- 504 Haubensack, C., 1981, Environnement des grès protérozoïques et des indices uranifères du
 505 secteur Kiéné dans le bassin de Franceville (République Gabonaise): aspects
 506 sédimentologiques et géochimiques.
- 507 Huang, H., Polat, A., and Fryer, B.J., 2013, Origin of Archean tonalite–trondhjemite–granodiorite
 508 (TTG) suites and granites in the Fiskenæsset region, southern West Greenland:
 509 Implications for continental growth: *Gondwana Research*, v. 23, p. 452-470.
- 510 Jackson, S.E., Pearson, N.J., Griffin, W.L., and Belousova, E.A., 2004, The application of laser
 511 ablation-inductively coupled plasma-mass spectrometry to in situ U–Pb zircon
 512 geochronology: *Chemical Geology*, v. 211, p. 47-69.
- 513 Lowell, J.D., and Guilbert, J.M., 1970, Lateral and vertical alteration-mineralization zoning in
 514 porphyry ore deposits: *Economic Geology*, v. 65, p. 373-408.
- 515 Martin, H., 1986, Effect of steeper Archean geothermal gradient on geochemistry of subduction-
 516 zone magmas: *Geology*, v. 14, p. 753-756.
- 517 Martin, H., 1987, Petrogenesis of Archean trondhjemites, tonalites, and granodiorites from
 518 eastern Finland: major and trace element geochemistry: *Journal of Petrology*, v. 28, p.
 519 921-953.
- 520 Martin, H., Moyen, J.-F., and Rapp, R., 2010, The sanukitoid series: magmatism at the
 521 Archean–Proterozoic transition, Sixth Hutton Symposium on the Origin of Granites and

- 522 Related Rocks: Proceedings of a Symposium Held in Stellenbosch, South Africa, 2-6 July
 523 2007, Volume 472, Cambridge Univ Press, p. 15.
- 524 Mathieu, R., 1999, Reconstitution des paléocirculations fluides et des migrations élémentaires
 525 dans l'environnement des réacteurs nucléaires naturels d'Oklo (Gabon) et des Argilites de
 526 Tournemire (France). : Thèse de Doctorat, Institut National Polytechnique, Lorraine, p.
 527 518.
- 528 Mathieu, R., Cuney, M., and Cathelineau, M., 2000, Geochemistry of palaeofluids circulation in
 529 the Franceville basin and around Oklo natural nuclear reaction zones (Gabon): JOURNAL
 530 OF GEOCHEMICAL EXPLORATION, v. 69, p. 245-249.
- 531 Mercadier, J., Richard, A., Boiron, M.-C., Cathelineau, M., and Cuney, M., 2010, Migration of
 532 brines in the basement rocks of the Athabasca Basin through microfracture networks (P-
 533 Patch U deposit, Canada): Lithos, v. 115, p. 121-136.
- 534 Muller, W., Shelley, M., Miller, P., and Broude, S., 2009, Initial performance metrics of a new
 535 custom-designed ArF excimer LA-ICPMS system coupled to a two-volume laser-ablation
 536 cell: Journal of Analytical Atomic Spectrometry, v. 24, p. 209-214.
- 537 Munoz, M., Boyce, A.J., Courjault-Rade, P., Fallick, A.E., and Tollon, F., 1999, Continental
 538 basinal origin of ore fluids from southwestern Massif central fluorite veins (Albigeois,
 539 France): evidence from fluid inclusion and stable isotope analyses: Applied
 540 Geochemistry, v. 14, p. 447-458.
- 541 Munz, I.A., Yardley, B.W.D., Banks, D.A., and Wayne, D., 1995, Deep penetration of
 542 sedimentary fluids in basement rocks from southern Norway: Evidence from hydrocarbon
 543 and brine inclusions in quartz veins: Geochimica et Cosmochimica Acta, v. 59, p. 239-
 544 254.
- 545 Murakami, T., Kasama, T., and Utsunomiya, S., 2011, Early Proterozoic weathering processes
 546 under low O₂ conditions reconstructed from a 2.45 Ga paleosol in Pronto, Canada: American
 547 Mineralogist, v. 96, p. 1613-1623.
- 548 Naudet, R., 1991, Des Réacteurs Nucléaires Fossiles: Paris (coll. CEA).
- 549 Nedachi, Y., Nedachi, M., Bennett, G., and Ohmoto, H., 2005, Geochemistry and mineralogy of
 550 the 2.45 Ga Pronto paleosols, Ontario, Canada: Chemical Geology, v. 214, p. 21-44.
- 551 Nesbitt, H.W., 1979, Mobility and fractionation of rare earth elements during weathering of a
 552 granodiorite: Nature, v. 279, p. 206-210.
- 553 Norman, D.K., Parry, W.T., and Bowman, J.R., 1991, Petrology and geochemistry of propylitic
 554 alteration at Southwest Tintic, Utah: Economic Geology, v. 86, p. 13-28.
- 555 Ohmoto, H., 1996, Evidence in pre-2.2 Ga paleosols for the early evolution of atmospheric
 556 oxygen and terrestrial biota: Geology, v. 24, p. 1135-1138.

- 557 Ohmoto, H., and Kerrick, D.M., 1977, Devolatilization equilibria in graphitic systems: American
558 Journal of Science, v. 277, p. 1013-1044.
- 559 Oliver, N.H.S., McLellan, J.G., Hobbs, B.E., Cleverley, J.S., Ord, A., and Feltrin, L., 2006, 100th
560 Anniversary Special Paper: Numerical Models of Extensional Deformation, Heat
561 Transfer, and Fluid Flow across Basement-Cover Interfaces during Basin-Related
562 Mineralization: Economic Geology, v. 101, p. 1-31.
- 563 Overstreet, W., 1960, Metamorphic grade and the abundance of ThO₂ in monazite: US
564 Geological Survey Professional Paper, p. 55-57.
- 565 Paquette, J.L., and Tiepolo, M., 2007, High resolution (5 µm) U–Th–Pb isotope dating of
566 monazite with excimer laser ablation (ELA)-ICPMS: Chemical Geology, v. 240, p. 222-
567 237.
- 568 Prian, J.P., and Johan, V., 1989, Contribution à la reconnaissance géologique et pétrographique
569 de l'Archéen du massif du Chaillu et du Francevillian du Bassin des Abeilles (région
570 deKoulamoutou – Lastoursville, Gabon): Rapport BRGM 89 GAB 079 GEO, v. 55 p.
- 571 Richard, A., Boulvais, P., Mercadier, J., Boiron, M.-C., Cathelineau, M., Cuney, M., and France-
572 Lanord, C., 2013, From evaporated seawater to uranium-mineralizing brines: Isotopic and
573 trace element study of quartz–dolomite veins in the Athabasca system: Geochimica et
574 Cosmochimica Acta, v. 113, p. 38-59.
- 575 Rye, R., and Holland, H.D., 1998, Paleosols and the evolution of atmospheric oxygen; a critical
576 review: American Journal of Science, v. 298, p. 621-672.
- 577 Sère, V., 1996, Géochimie des minéraux néoformés à Oklo (Gabon): histoire géologique du
578 bassin d'Oklo, une contribution pour les études de stockages géologiques de déchets
579 radioactifs: Thèse de Doctorat, Université de Paris VII, p. 278.
- 580 Seydoux-Guillaume, A.-M., Paquette, J.-L., Wiedenbeck, M., Montel, J.-M., and Heinrich, W.,
581 2002, Experimental resetting of the U–Th–Pb systems in monazite: Chemical Geology, v.
582 191, p. 165-181.
- 583 Smith, H., and Barreiro, B., 1990, Monazite U-Pb dating of staurolite grade metamorphism in
584 pelitic schists: Contributions to Mineralogy and Petrology, v. 105, p. 602-615.
- 585 Stern, R., 1989, Petrogenesis of the Archean sanukitoid suite: State university at Stony Brook,
586 New York, p. 275 p.
- 587 Thiéblemont, D., Castaing, C., Billa, M., Bouton, P., and and Préat, A., 2009, Notice explicative
588 de la Carte géologique et des Ressources minérales de la République Gabonaise à 1/1000
589 000: Editions DGMG - Ministère des Mines, du Pétrole, des Hydrocarbures, Libreville, p.
590 384.
- 591 Thomas, R.J., Makanga, J.F., and Chevallier, L., 2001, Carte géologique de la République
592 Gabonaise à 1/ 1 000 000: 2eme Editions, DGMG Gabon.

- 593 Titley, S.R., Thompson, R.C., Haynes, F.M., Manske, S.L., Robison, L.C., and White, J.L., 1986,
 594 Evolution of fractures and alteration in the Sierrita-Esperanza hydrothermal system, Pima
 595 County, Arizona: Economic Geology, v. 81, p. 343-370.
- 596 Velde, B., and Meunier, A., 2008, The Origin of Clay Minerals in Soils and Weathered Rocks:
 597 With 23 Tables, Springer.
- 598 Weber, F., 1968, Une série précambrienne du Gabon, le Francevillian: sédimentologie,
 599 géochimie, relations avec les gîtes minéraux associés, Université de Strasbourg.
- 600 Weber, F., and Gauthier-Lafaye, F., 2013, No proof from carbon isotopes in the Francevillian
 601 (Gabon) and Onega (Fennoscandian shield) basins of a global oxidation event at 1980–
 602 2090 Ma following the Great Oxidation Event (GOE): Comptes Rendus Geoscience, v.
 603 345, p. 28–35.
- 604 White, A.F., Bullen, T.D., Schulz, M.S., Blum, A.E., Huntington, T.G., and Peters, N.E., 2001,
 605 Differential rates of feldspar weathering in granitic regoliths: Geochimica et
 606 Cosmochimica Acta, v. 65, p. 847–869.
- 607 Wing, B., Ferry, J., and Harrison, T.M., 2003, Prograde destruction and formation of monazite
 608 and allanite during contact and regional metamorphism of pelites: petrology and
 609 geochronology: Contributions to Mineralogy and Petrology, v. 145, p. 228–250.
- 610

611 **Figure captions**

- 612
- 613 **Fig. 1:** Simplified geological map of Franceville basin and location of the studied region
 614 (modified after Bros et al, 1993).
- 615
- 616 **Fig. 2:** (a) Location of the studied drill cores (KA13, GR1, GR5, GR20, GR23, GR31, GR 43 and
 617 KA6) close to Kaya-Kaya fault in the Franceville basin; (b) Simplified geological logs of the
 618 studied drill cores.
- 619
- 620 **Fig. 3:** Bulk rock chemical compositions in the Debon and Le Fort diagram (1983). In brackets
 621 (L.O.I.), Q = normative quartz, P = normative feldspars. (a) GR20 and GR31 drill cores, (b)
 622 GR23, KA6 drill cores. Dot arrow = magmatic differentiation trend. The white triangles represent
 623 the average compositions of the diorite quartzite (dq), tonalite (to), granodiorites (gd), and
 624 adamellite (ad)
- 625

626 **Fig. 4:** Chondrite-normalized rare earth element patterns of the least altered rocks.
 627 Adamellite(KA6 472), Granodiorite (KA6 445, GR31 873 and GR31 866), Tonalite (KA6 467,
 628 KA6 454, KA6 449, KA6 444, KA6 438, GR23 640), Diorite (KA6 462).

629
 630 **Fig. 5:** Photomicrographs of the granitoids affected by propylitic alteration: (a) biotite is
 631 completely replaced by the chlorite associated to rod shaped allanite and titanite, backscattered
 632 electron SEM image; (b) sericitization of the feldspar, chloritization of biotite and chlorite calcite
 633 sequence of fissure infilling. chloritized biotite = chl biot, chlorite = chl, allanite = All, titanite =
 634 tin, feldspar = Felds, calcite = Cal, QZ = quartz.

635
 636 **Fig. 6:** Photomicrographs of illitization features in granitoids; (a) feldspars are completely
 637 replaced by illite while quartz (Qz) are cracked and enveloped by illitic matrix; (b) The
 638 chloritized biotite is partially to totally replaced by the Fe-oxide + phengite (Phg) assemblage; (c)
 639 fracture filled by calcite (cal); (d) Cementation in the FA sandstone by anhydrite.

640
 641 **Fig. 7:** Evolution of Δ LOI with depth of tonalite.

642
 643 **Fig. 8:** Plot of ΔSiO_2 , $\Delta\text{Al}_2\text{O}_3$, ΔCaO , $\Delta\text{Na}_2\text{O}$, $\Delta\text{Fe}_2\text{O}_3$, ΔMgO , $\Delta\text{K}_2\text{O}$ versus ΔLOI of
 644 propylitized (black diamond) and illitized (open circle) tonalite.

645 **Fig. 9:** Plot of ΔRb , ΔSr , ΔLa , ΔCe , ΔCs , ΔTh , ΔU versus ΔLOI of propylitized (black diamond)
 646 and illitized (open circle) tonalites.

647
 648 **Fig. 10:** Evolution of the chondrite-normalized rare earth element patterns of the granitoids, from
 649 the least altered to the most altered (illitized) granitoids. Open square = illitized granitoids, black
 650 losange = superimposed illitic on propylitic alteration, open circle = least altered and propylitized
 651 granitoids.

652
 653 **Fig. 11:** (a) Evolution of the XRD patterns of the $< 2 \mu\text{m}$ fractions from KA6 467 m (granitoids)
 654 to KA6 436 m (sandstone); (b) Evolution of the XRD patterns of chlorite from KA6 467 m
 655 tonalite), to KA6 438 drill core $< 2\mu\text{m}$ fraction in oriented glycol saturation preparations. Chl =
 656 chlorite, ill = illite.

657
 658 **Fig. 12:** (a) Representation of the four clay mineral domains in the MR^{3+} , 2R^{3+} , 3R^{2+} triangle
 659 (Velde, 1985): illite, phengite (Ph), chlorite upper zone (chl_{up}) and chlorite lower zone (chl_{low}),
 660 phengite + chlorite mixture (Ph + chl_{up}) domain. (b) Evolution of chemical compositions of the
 661 chlorites analyzed from the depth (lower zone) to the unconformity (upper zone) in the Fe/(Fe +
 662 Mg) versus Si diagram. Open diamond = chlorite of lower zone, open circles = chlorite of upper
 663 zone.

664
 665 **Fig. 13:** Representation of Pb and U isotopic data in the $^{206}\text{Pb}/^{238}\text{U}$ versus $^{207}\text{Pb}/^{235}\text{U}$ diagram.
 666 MSWD = Mean Square Weighted Deviation. Monazites of KA6 437.85 sample.

667
 668 **Fig. 14:** Representation of Pb and U isotopic data $^{207}\text{Pb}/^{206}\text{Pb}$ versus $^{206}\text{Pb}/^{238}\text{U}$ diagram. MSWD
 669 = Mean Square Weighted Deviation. Monazites of GR1 631 sample.

670
 671 **Fig. 15:** (a) Representation of the alteration effects in the Al_2O_3 - CaO^* + Na_2O + K_2O - FeO +
 672 MgO diagrams (Rainbird et al., 1990). CaO^* = CaO of silicates. L.alt = least altered rocks, Pro +
 673 dif = propylitized rocks + magmatic differentiation, Ill. = analyzed illites, phg = analyzed
 674 phengites. Illite = theoretical illite, Ka = kaolinite, Gi = Gibbsite. Black arrows indicate the least
 675 altered rock to-propylitized rock and the propylitized rock-to- illitized rock. (1) 2.6 Ga propylitic
 676 event, (2) 1.87 Ga late diagenetic (illitic) event.

677
 678 **Table captions**

680 **Table 1:** Whole-rock geochemical data for the Archean granitoids at Kiéné area.

681
 682 **Table 2:** Representative microprobe analyses of chlorites from the propylitic zone. The structural
 683 formulae are calculated on the 14 oxygen basis.

684
 685 **Table 3:** Representative microprobe analyses of chlorites from the illitic zone. The structural
 686 formulae are calculated on the 14 oxygen basis.

688 **Table 4:** Representative microprobe analyses of phengites from 797 the illitic zone. The
689 structural formulae are calculated on the 11 oxygen basis.

690

691 **Table 5:** Representative microprobe analyses of illites from the illitic zone. The structural
692 800 formulae are calculated on the 11 oxygen basis.

693

694 **Table 6:** Representative microprobe analyses of epidotes and allanites from the propylitic zone.
695 The structural formulae are calculated on the 12.5 oxygen basis.

696

697 **Table 7:** Representative microprobe analyses of monazites.

698

699 **Table 8:** Representative Laser-ICPMS analyses and age calculations of monazites (sample
700 805 KA6 437.85).

701

702 **Table 9:** Representative Laser-ICPMS analyses and age calculations of monazites (sample
703 807 GR1 631).

704

705 **Table 10:** $\delta^{13}\text{C}$ values (‰ PDB) and $\delta^{18}\text{O}$ (‰ SMOW) measured on six samples affected by
706 carbonated alteration.

707

708

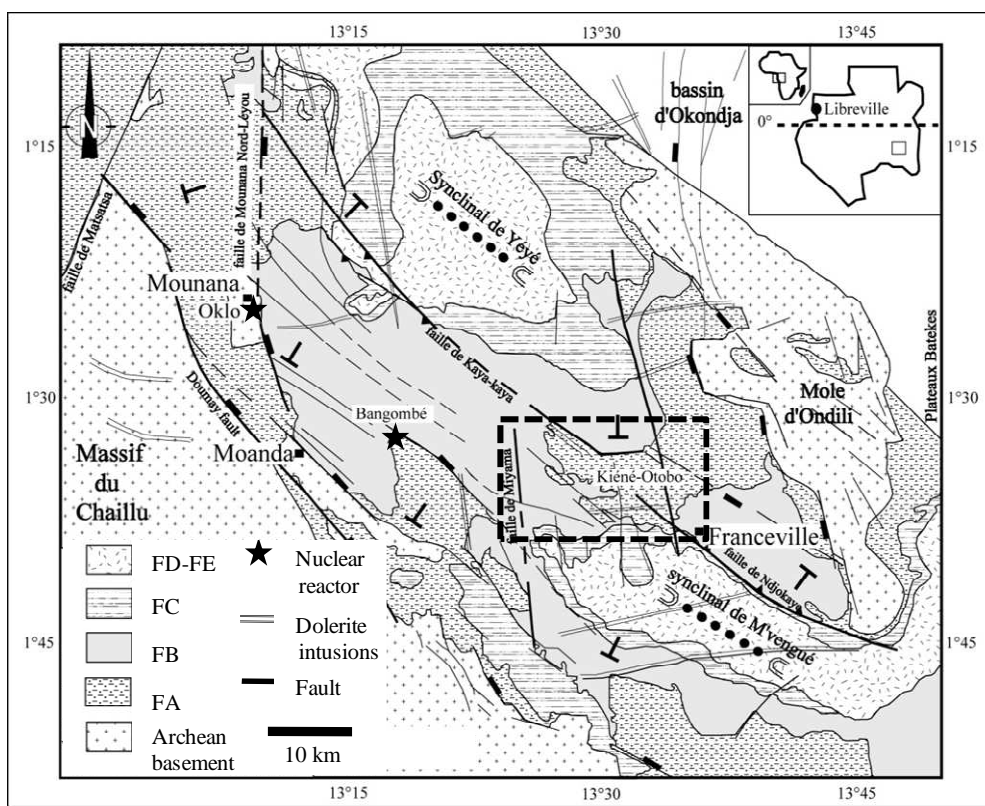


Figure 1

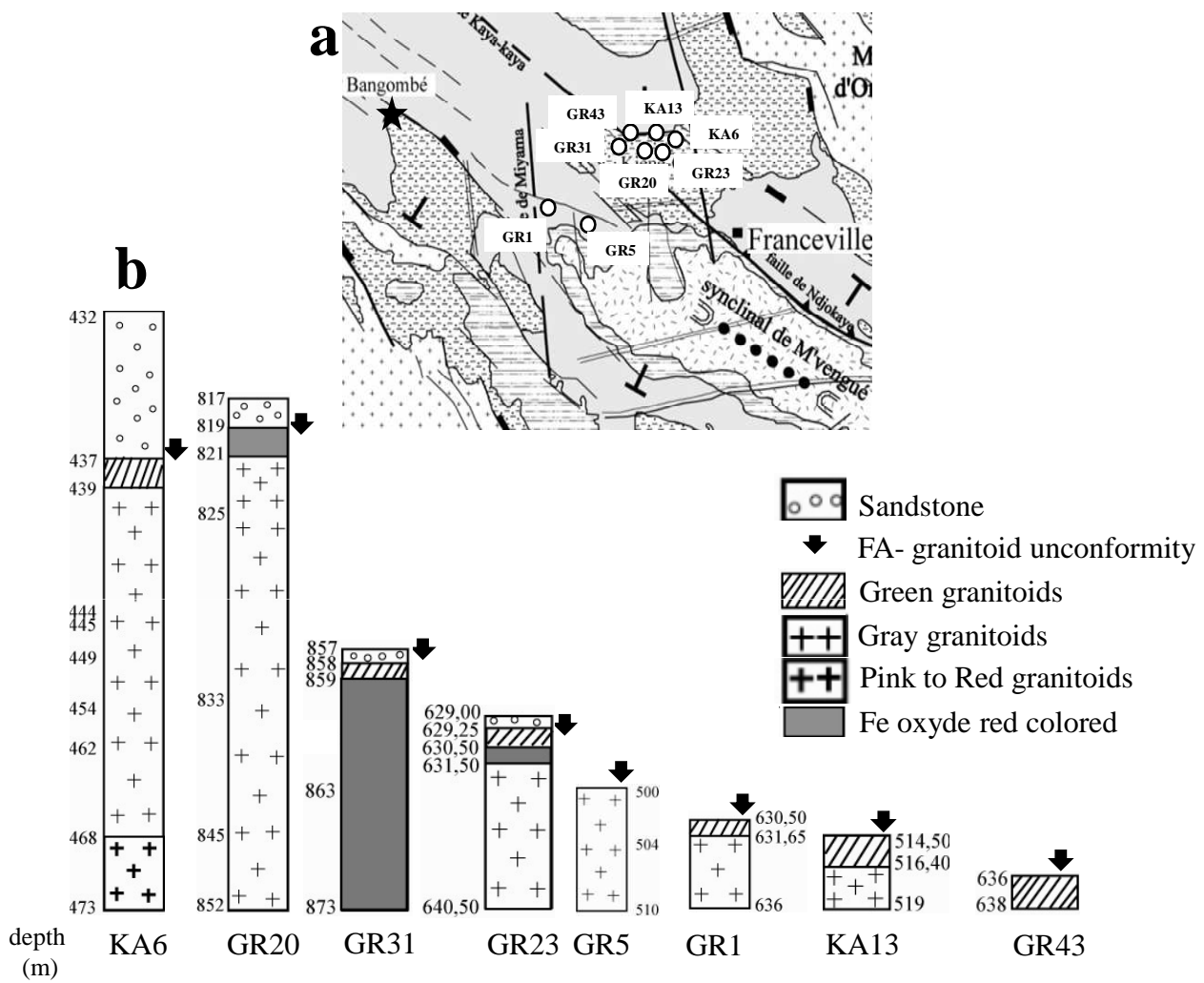


Figure 2

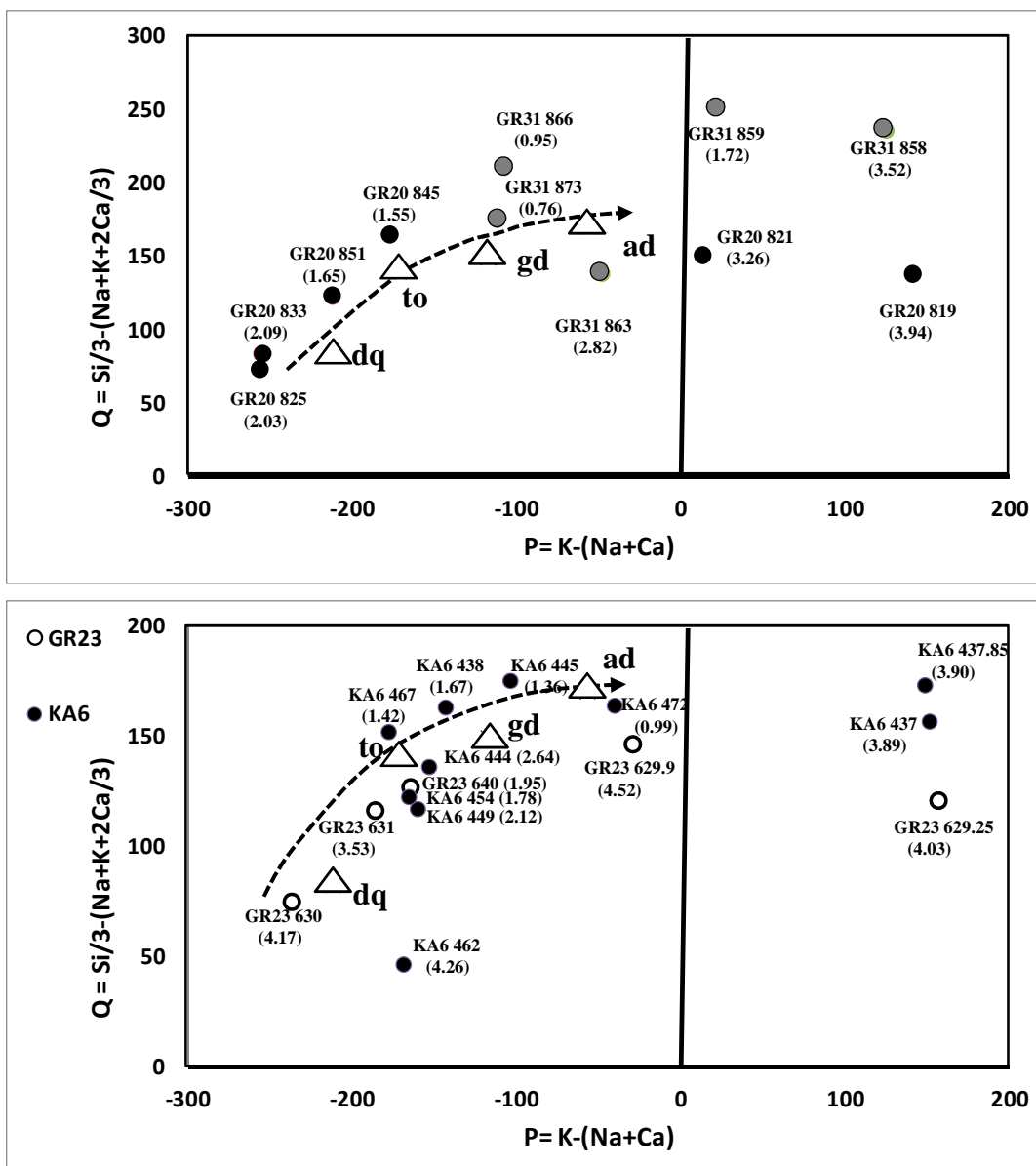


Figure 3

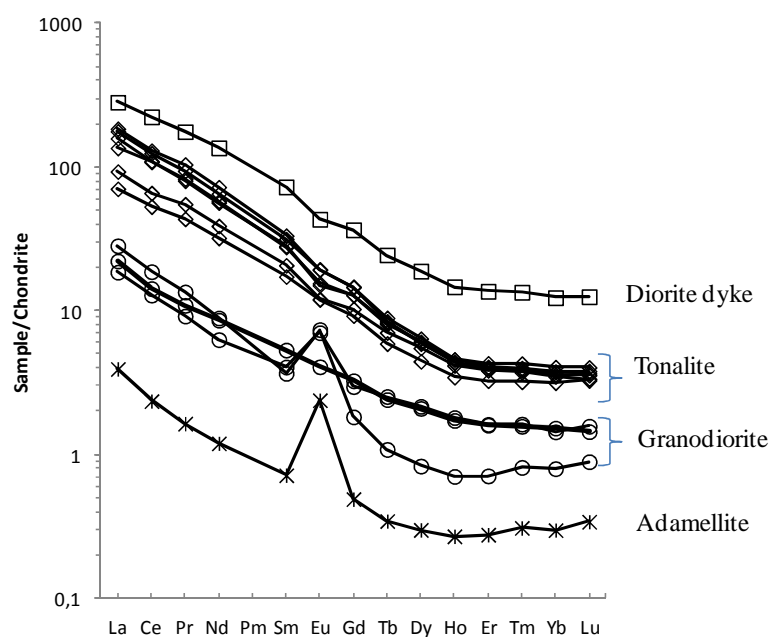


Figure 4

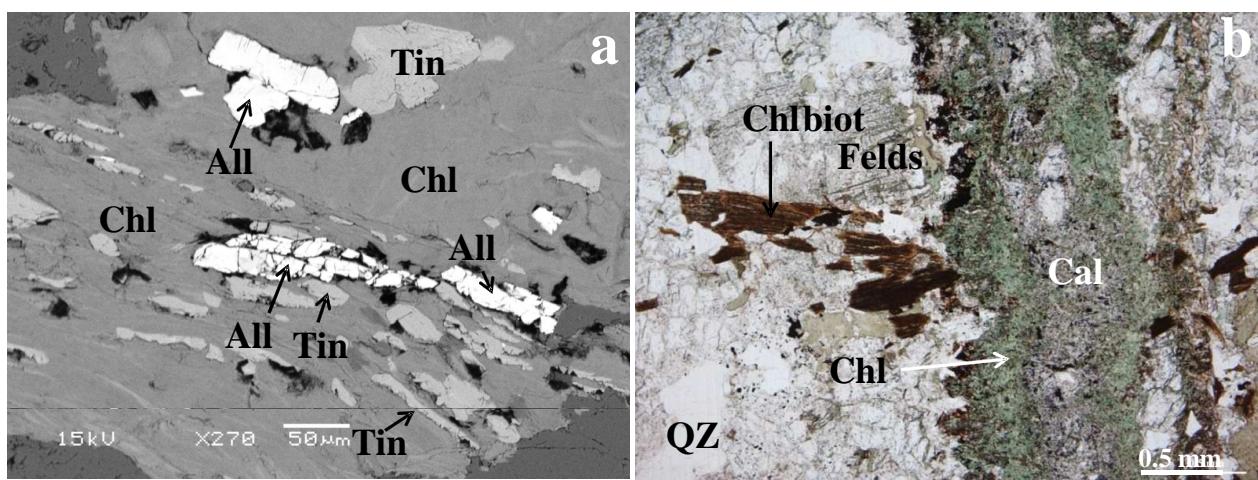


Figure 5

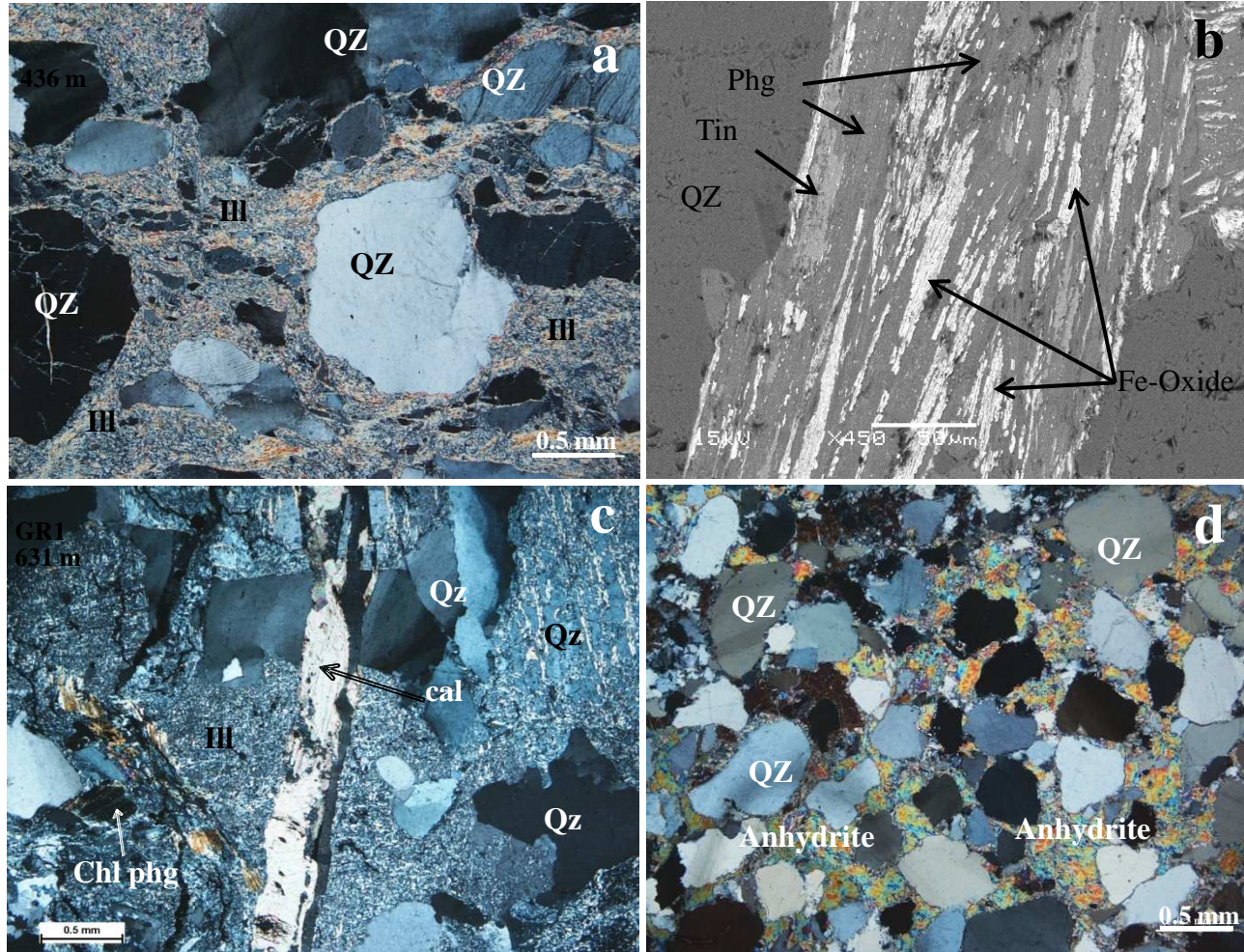


Figure 6

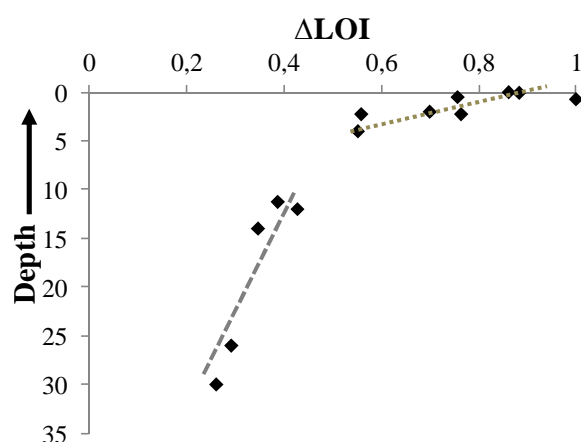


Figure 7

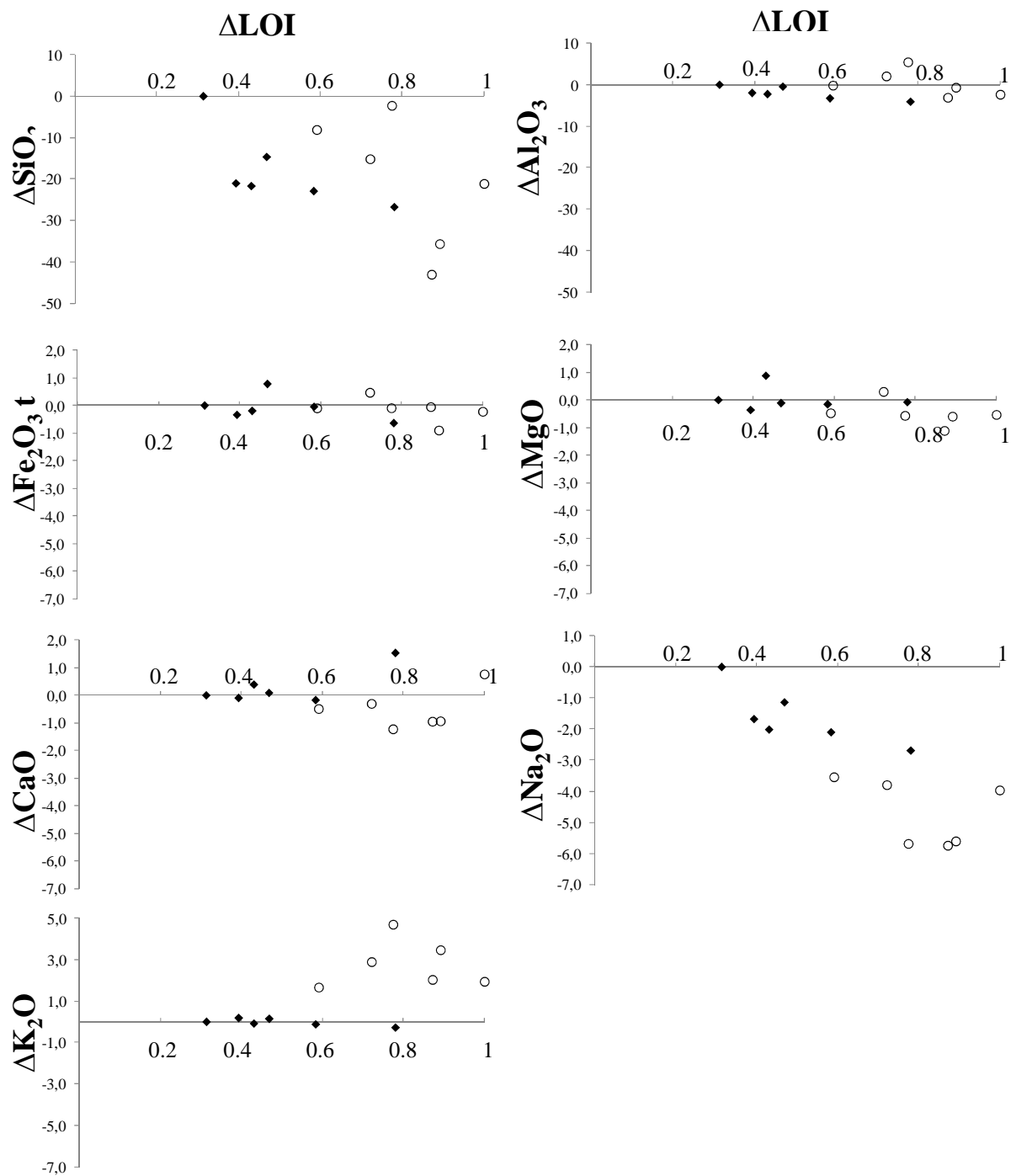


Figure 8

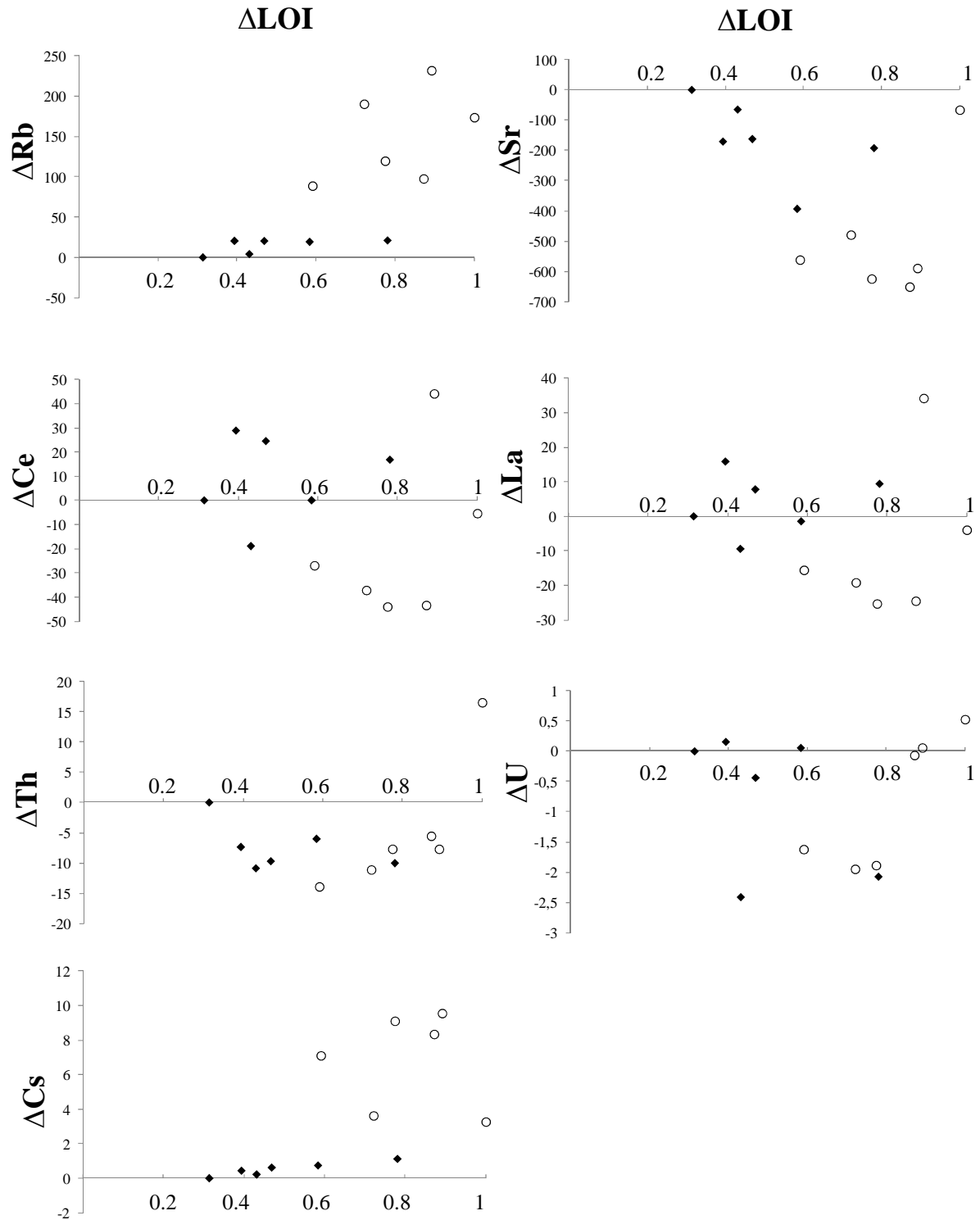


Figure 9

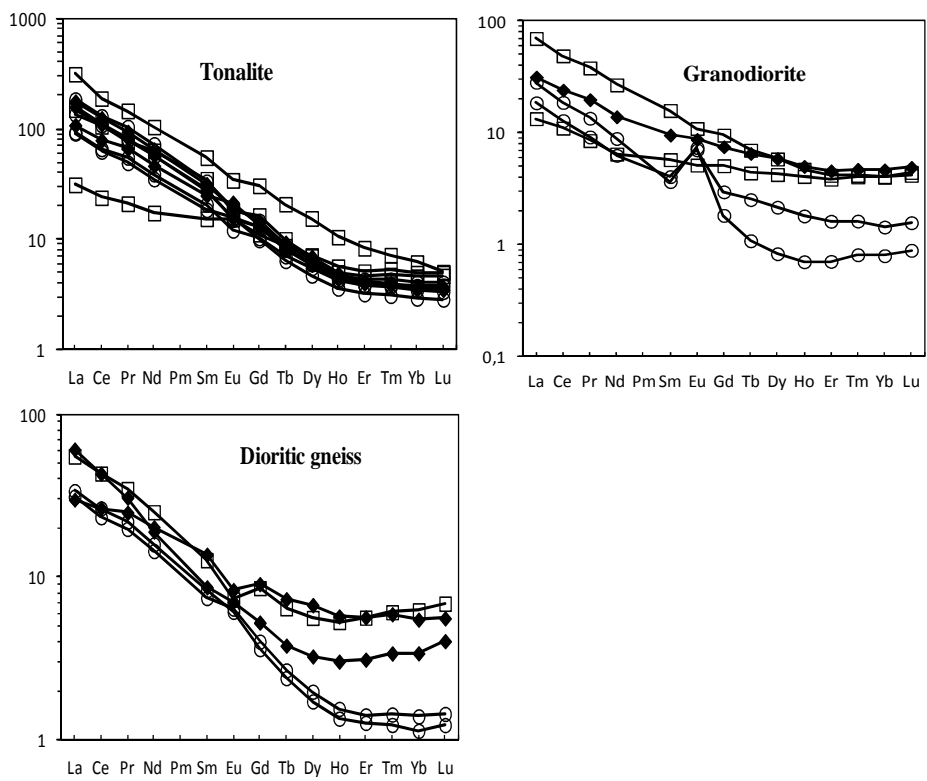


Figure 10

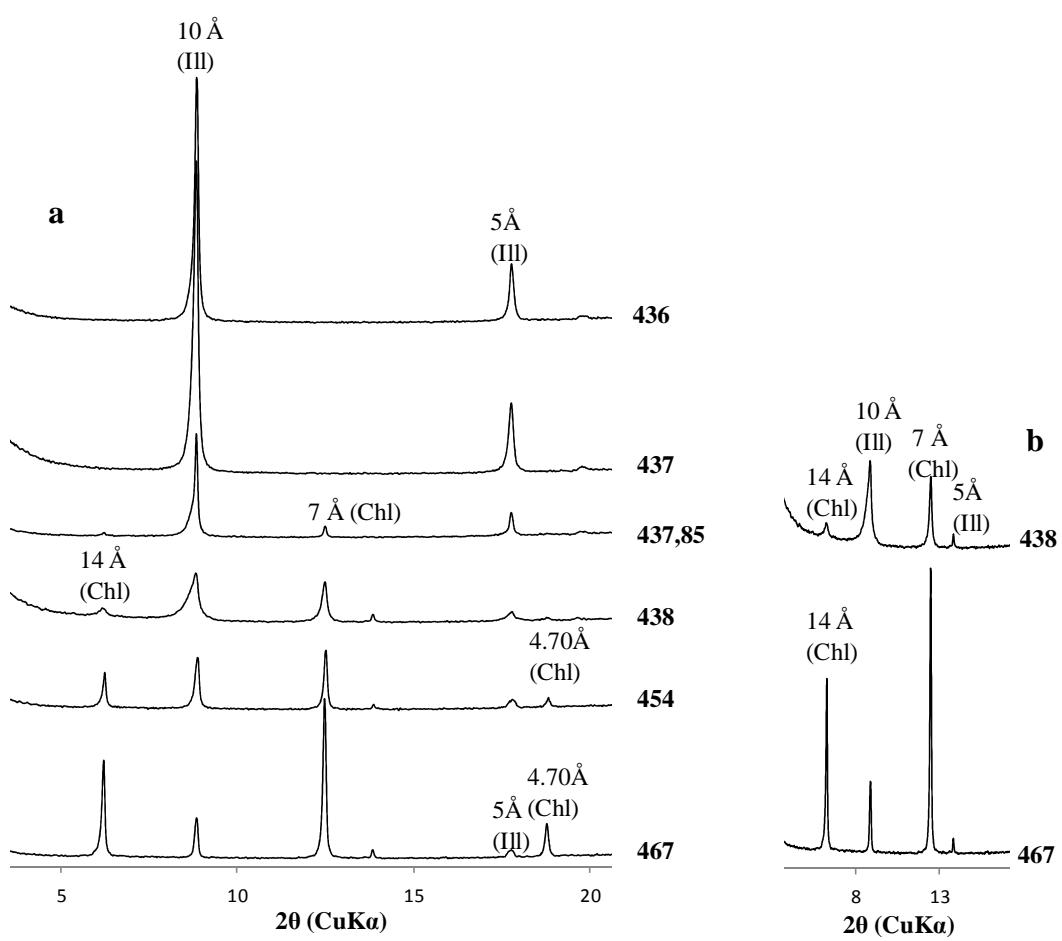
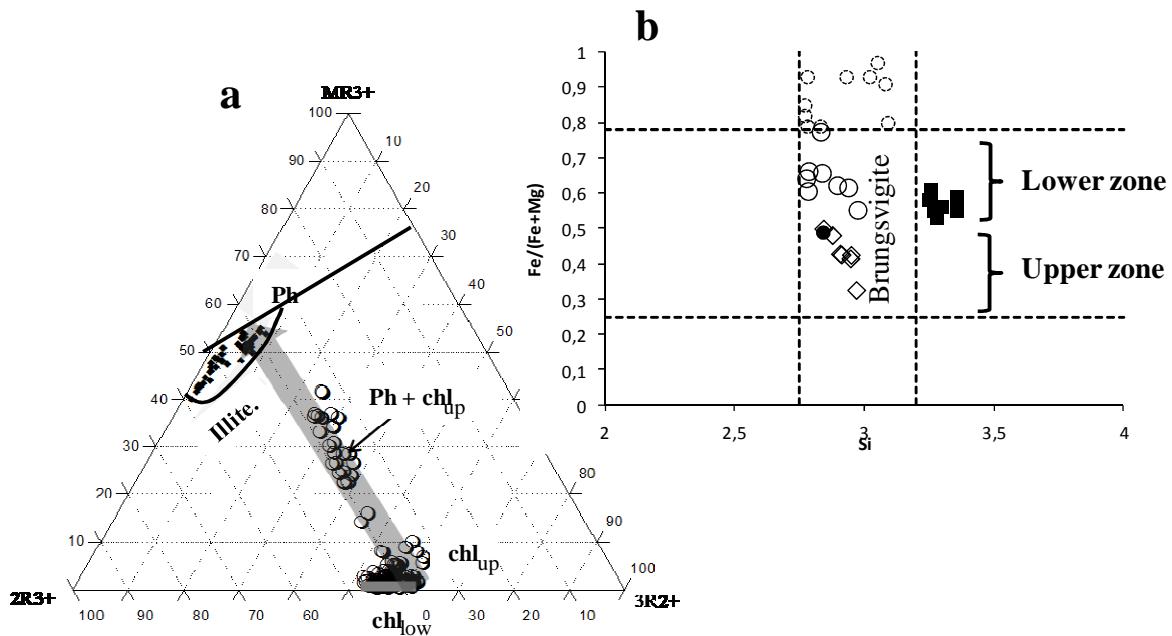


Figure 11



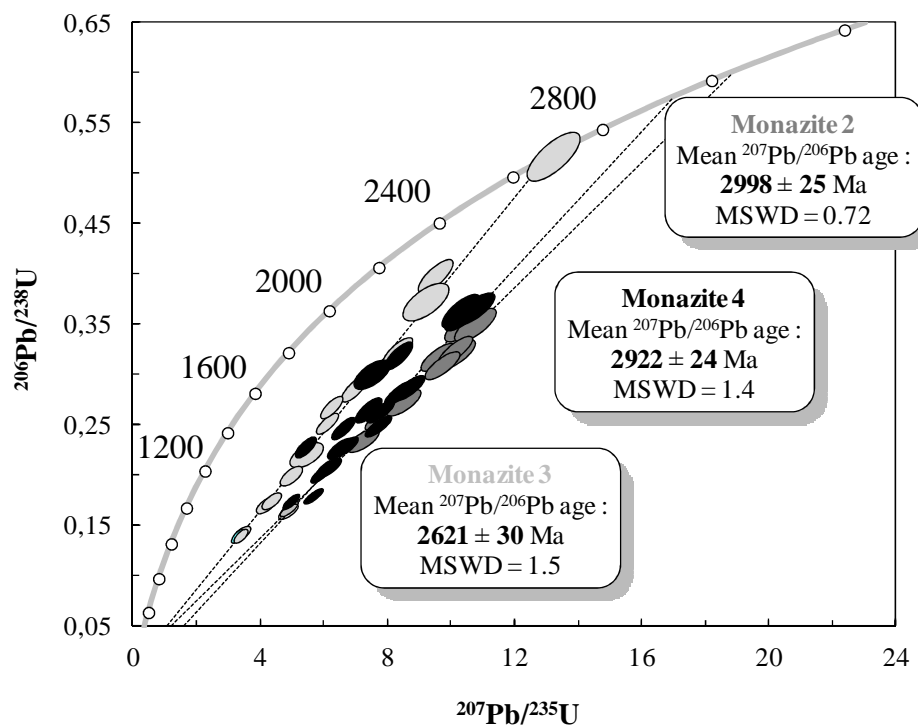


Figure 13

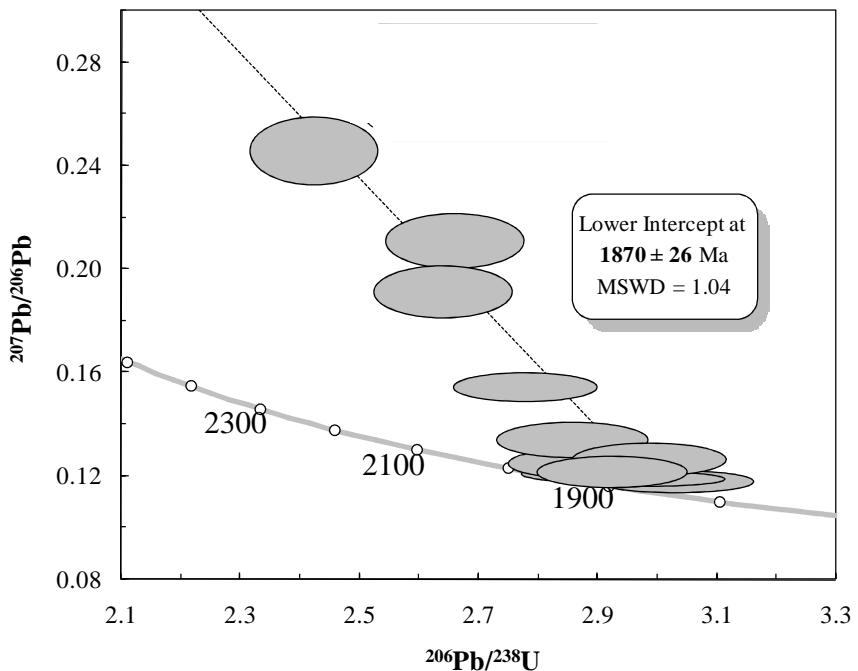


Figure 14

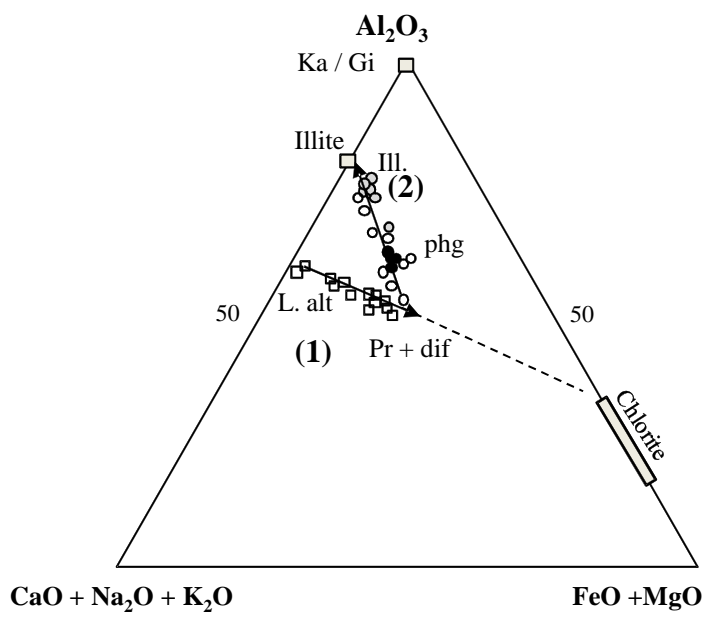


Figure 15

Table 1

	Granitoid					Sandstone			Granitoid					Sandstone	
	GR23 640,50	GR23 631,50	GR23 630,90	GR23 629,90	GR23 629,25	GR23 629,18	GR20 851	GR20 845	GR20 833	GR20 825	GR20 821	GR20 819	GR20 818	GR20 818	
SiO ₂ (Wt%)	64,74	63,91	61,72	63,42	57,00	70,17	69,05	68,08	56,74	60,99	62,10	55,55	75,20		
TiO ₂	0,45	0,50	0,39	0,44	0,56	0,09	0,30	0,19	0,32	0,52	0,38	0,70	0,07		
Al ₂ O ₃	16,15	15,07	15,81	15,58	22,83	5,17	15,35	16,49	18,45	17,66	18,62	23,36	5,04		
FeOt	4,23	4,01	3,93	4,07	4,08	0,87	2,65	1,86	8,16	4,71	4,33	6,86	0,62		
MnO	0,05	0,06	0,07	0,02	0,02	0,00	0,03	0,02	0,06	0,07	0,04	0,01	0,00		
MgO	3,15	2,05	1,88	1,22	1,46	0,31	1,79	0,89	1,61	2,06	2,01	0,73	0,26		
CaO	2,24	4,19	5,07	2,67	0,58	8,17	2,03	3,07	6,68	5,32	1,12	0,69	6,50		
Na ₂ O	5,13	4,66	5,49	2,42	0,35	0,07	5,21	5,84	4,66	5,46	2,30	0,14	0,03		
K ₂ O	1,89	1,80	1,42	4,50	8,34	2,32	1,23	1,43	0,59	0,71	5,01	7,38	1,68		
P ₂ O ₅	0,23	0,26	0,23	0,27	0,03	0,00	0,10	0,08	0,07	0,14	0,08	0,19	0,04		
LOI	1,95	3,53	4,17	4,52	4,03	12,20	1,65	1,55	2,09	2,03	3,26	3,94	9,10		
Total	100,20	100,03	100,18	99,12	99,25	99,37	99,38	99,50	99,41	99,67	99,24	99,55	98,55		
Ba(ppm)	1060,00	1147,00	476,40	4229,00	1700,00	830,40	401,20	622,10	243,70	388,30	2552,00	831,90	469,50		
Rb	40,77	70,11	61,46	261,50	433,60	107,80	30,21	32,20	15,80	17,39	247,00	259,20	62,30		
Sn	1,12	1,18	1,07	0,97	1,91	0,32	0,59	0,00	0,91	1,16	0,87	1,93	0,31		
Sr	802,90	695,90	533,40	775,50	115,50	780,00	490,10	738,60	1293,00	573,20	204,50	15,23	385,50		
Ga	21,62	21,71	20,30	20,46	33,50	6,43	17,50	17,85	26,20	22,31	23,63	29,91	6,09		
Y	9,72	11,63	11,09	12,01	25,19	7,12	3,76	3,66	9,05	14,35	7,46	13,02	3,71		
Zr	141,80	179,50	137,30	155,50	221,00	337,00	59,26	100,80	368,40	158,80	32,17	286,50	124,20		
Nb	4,07	3,61	2,83	3,54	7,49	2,29	2,10	1,32	1,04	3,62	2,73	7,48	1,83		
Cs	0,50	1,89	1,43	4,49	16,31	1,52	0,42	0,33	0,33	0,27	4,32	17,79	3,04		
Cu	0,00	47,83	93,11	20,02	8,18	10,75	7,91	23,41	5,25	15,86	39,96	4,06	22,26		
Zn	67,14	66,51	99,82	93,88	81,95	19,63	43,66	33,26	76,97	66,83	110,70	39,94	15,07		
Hf	3,59	4,34	3,35	3,82	5,39	7,78	1,63	2,87	8,81	3,82	1,00	6,99	3,17		
Ta	0,26	0,23	0,20	0,44	0,45	0,25	0,14	0,08	0,11	0,35	0,20	0,42	0,17		
Pb	7,20	42,63	381,32	23,23	19,27	5,44	6,62	10,64	8,72	10,26	3,24	8,25	1,93		
Th	5,68	7,55	2,20	41,43	12,45	11,86	2,85	0,62	7,52	1,16	4,56	20,04	6,45		
U	0,50	1,05	1,31	4,33	4,78	3,59	0,57	0,52	2,50	0,34	0,95	5,69	1,22		
V	64,36	74,24	70,28	62,46	256,10	146,40	40,54	14,51	80,11	73,27	51,95	84,92	19,92		
La	33,46	65,07	58,12	39,61	114,90	14,42	11,47	12,42	22,37	11,01	17,16	20,31	3,40		
Ce	59,83	119,40	105,20	75,67	180,30	24,56	22,37	25,32	41,44	25,44	29,71	41,50	5,93		
Pr	6,76	12,87	11,33	9,08	19,94	3,15	2,71	3,01	4,23	3,42	3,42	4,77	0,75		
Nd	24,99	46,31	41,11	32,99	74,04	12,13	10,30	11,32	13,56	14,44	2,73	17,84	2,85		
Sm	4,28	7,29	6,41	5,78	12,69	2,40	1,72	1,92	2,00	3,18	2,85	2,94	0,60		
Eu	1,36	1,68	1,35	1,87	2,98	0,66	0,56	0,53	0,61	0,73	0,90	0,64	0,21		
Gd	3,02	4,46	3,94	4,15	9,36	1,84	1,23	1,11	1,61	2,77	2,15	2,62	0,70		
Tb	0,37	0,52	0,48	0,54	1,21	0,24	0,16	0,14	0,22	0,43	0,30	0,37	0,10		
Dy	1,80	2,44	2,25	2,65	5,90	1,19	0,75	0,66	1,24	2,57	1,64	2,14	0,63		
Ho	0,31	0,39	0,37	0,42	0,89	0,22	0,13	0,12	0,26	0,49	0,29	0,45	0,12		
Er	0,80	1,02	0,99	1,05	2,07	0,67	0,35	0,32	0,78	1,41	0,77	1,41	0,34		
Tm	0,11	0,14	0,14	0,14	0,26	0,10	0,05	0,04	0,12	0,21	0,11	0,22	0,05		
Yb	0,72	0,93	0,89	0,87	1,53	0,78	0,16	0,14	0,22	1,36	0,72	0,37	0,34		
Lu	0,11	0,14	0,14	0,13	0,19	0,14	0,06	0,05	0,15	0,21	0,10	0,26	0,06		

Table 1 (Continued)

	Granitoid					Sandstone GR31 857	Granitoid					Sandstone					
	GR31 873	GR31 866	GR31 863	GR31 859	GR31 858		KA6 472	KA6 467,90	KA6 462	KA6 454	KA6 449	KA6 445,60	KA6 444	KA6 438,7	KA6 437,85	KA6 437	KA6 432
SiO ₂ (Wt %)	73,73	74,47	62,19	73,33	66,75	86,53	73,68	69,54	52,11	65,63	65,07	74,17	65,20	71,01	60,91	56,67	92,05
TiO ₂	0,14	0,23	0,62	0,13	0,21	0,09	0,04	0,33	0,99	0,45	0,40	0,04	0,47	0,42	0,61	0,87	0,05
Al ₂ O ₃	14,68	12,78	17,78	14,37	20,33	6,78	13,92	14,18	17,26	16,52	16,27	13,81	15,24	15,27	22,43	22,71	3,92
FeOt	1,76	2,80	5,46	2,39	1,44	0,70	0,30	3,32	9,41	4,03	4,86	0,47	4,58	2,40	2,76	6,20	0,20
MnO	0,02	0,02	0,10	0,01	0,03	0,01	0,01	0,03	0,09	0,03	0,04	0,01	0,05	0,02	0,01	0,03	0,00
MgO	0,38	0,43	2,38	0,74	0,59	0,27	0,17	1,45	3,50	1,47	1,59	0,16	1,82	0,66	0,91	1,67	0,10
CaO	1,14	1,21	0,75	0,32	0,16	0,44	0,89	1,27	4,26	1,59	1,61	1,47	1,53	1,75	0,42	0,06	0,04
Na ₂ O	4,85	4,27	3,61	1,93	0,09	0,05	4,03	5,81	4,43	5,59	5,53	4,61	5,18	5,00	0,07	0,09	0,12
K ₂ O	3,02	2,39	3,82	4,18	6,11	2,19	4,92	1,48	2,32	2,25	1,93	3,31	1,90	2,29	7,40	7,25	1,97
P ₂ O ₅	0,03	0,08	0,19	0,03	0,03	0,06	0,00	0,19	0,82	0,23	0,23	0,00	0,21	0,22	0,28	0,03	0,00
LOI	0,76	0,95	2,82	1,72	3,52	1,77	0,99	1,42	4,26	1,78	2,12	1,36	2,64	1,67	3,90	3,89	0,51
Total	100,51	99,61	99,72	99,14	99,24	98,88	98,93	99,02	99,44	99,57	99,63	99,40	98,81	100,71	99,69	99,47	98,95
Ba(ppm)	1014,00	740,50	577,10	874,60	538,40	1800,00	3861,00	976,40	1355,00	2100,00	1551,00	5313,00	1109,00	990,40	2007,00	2237,00	543,70
Rb	61,78	60,31	194,40	182,50	168,60	74,69	95,06	25,94	70,29	62,86	54,99	59,19	63,20	71,04	246,80	252,40	59,84
Sn	0,62	0,72	1,54	0,58	0,75	0,00	0,00	1,05	2,07	1,20	1,33	0,00	3,23	0,89	3,45	1,89	0,00
Sr	222,40	202,30	121,80	59,10	15,89	131,80	553,80	658,20	643,50	659,70	587,60	634,60	370,10	586,30	57,23	52,65	32,24
Ga	17,28	17,18	24,91	20,08	26,15	8,77	13,20	16,31	24,81	22,77	23,01	14,97	23,95	18,14	31,57	28,22	4,31
Y	4,62	13,04	8,68	12,32	11,28	3,97	0,80	9,95	35,31	11,16	11,25	2,02	9,67	8,55	11,46	15,69	2,11
Zr	57,04	165,80	110,60	97,47	167,30	47,66	16,28	120,30	234,30	154,00	146,90	50,36	160,50	150,50	218,10	262,70	59,63
Nb	2,91	5,71	3,92	2,97	5,50	1,34	0,21	3,61	8,33	5,07	5,08	0,23	5,39	4,86	6,21	10,41	1,31
Cs	0,55	0,71	3,40	2,72	8,01	4,47	0,55	0,15	1,85	0,79	0,91	0,39	1,25	2,14	15,50	7,05	1,10
Cu	6,54	11,37	34,02	4,29	0,00	12,30	8,30	17,85	65,30	42,13	18,92	123,80	41,43	0,00	0,00	0,00	5,55
Zn	30,30	41,49	268,60	74,10	59,29	29,28	0,00	46,25	130,00	50,28	62,36	0,00	58,56	32,64	39,11	73,37	0,00
Hf	1,61	4,71	3,05	3,43	5,39	1,33	0,38	2,96	5,47	3,79	3,65	1,60	3,98	3,63	5,42	6,92	1,63
Ta	0,15	0,35	0,27	0,08	0,24	0,12	0,01	0,21	0,47	0,33	0,34	0,02	0,34	0,43	0,67	1,00	0,13
Pb	7,25	6,66	5,70	10,27	3,43	2,07	8,99	4,04	29,46	45,59	16,15	10,68	45,39	88,14	5,57	10,07	4,50
Th	1,38	8,79	2,09	4,37	9,97	4,13	0,77	15,08	17,55	10,46	6,38	0,67	12,69	8,79	7,52	24,00	3,45
U	0,51	0,89	1,49	1,99	2,78	1,35	0,23	2,78	4,98	3,97	2,78	0,61	3,97	4,83	2,83	12,94	0,60
V	10,49	18,94	79,74	67,65	14,88	14,27	4,92	86,66	199,90	116,20	128,40	4,08	88,59	37,92	54,50	75,21	2,50
La	6,82	11,55	14,41	25,61	4,92	17,36	1,45	34,16	103,70	67,71	49,74	10,40	45,73	25,89	55,00	11,44	11,30
Ce	12,31	23,10	28,22	46,72	10,56	28,32	2,25	63,12	213,90	124,50	103,90	17,91	88,34	50,81	101,30	22,80	16,67
Pr	1,26	2,72	3,44	5,22	1,17	3,49	0,23	7,55	24,13	14,27	11,01	1,85	9,58	5,97	10,45	2,88	1,99
Nd	2,91	5,71	3,92	2,97	4,60	11,81	0,85	27,66	96,64	51,54	40,18	6,34	5,39	22,82	45,21	12,33	6,61
Sm	0,94	2,21	2,96	3,66	1,33	2,07	0,17	4,79	16,82	7,69	6,53	0,85	6,65	3,99	8,11	3,55	0,90
Eu	0,61	0,76	0,89	0,95	0,45	0,52	0,21	3,15	11,24	4,50	3,93	0,56	1,21	2,83	1,57	1,33	0,21
Gd	0,91	2,30	2,69	2,92	1,56	1,65	0,15	0,41	1,42	0,49	0,47	0,06	4,01	0,34	5,05	3,41	0,55
Tb	0,15	0,38	0,35	0,41	0,25	0,20	0,02	2,10	7,20	2,27	2,32	0,32	0,46	1,70	0,58	0,50	0,07
Dy	0,83	2,24	1,78	2,23	1,62	0,86	0,11	2,10	7,20	2,27	2,32	0,32	2,14	1,70	2,67	2,73	0,38
Ho	0,15	0,43	0,27	0,40	0,35	0,13	0,02	0,35	1,25	0,37	0,39	0,06	0,34	0,29	0,43	0,48	0,06
Er	0,40	1,14	0,62	1,04	0,96	0,30	0,07	0,96	3,40	0,97	1,08	0,18	0,91	0,81	1,15	1,27	0,19
Tm	0,06	0,17	0,08	0,15	0,14	0,04	0,01	0,13	0,48	0,14	0,15	0,03	0,13	0,11	0,17	0,19	0,03
Yb	0,36	1,16	0,47	0,99	1,01	0,24	0,07	0,87	3,06	0,94	1,01	0,20	0,83	0,78	1,14	1,23	0,17
Lu	0,06	0,19	0,07	0,16	0,17	0,04	0,01	0,13	0,48	0,15	0,15	0,03	0,12	0,13	0,18	0,19	0,03

Table 2

	Chlorite in the propylitic zone								
SiO ₂ (Wt %)	27,42	27,33	27,19	28,99	28,69	31,08	28,79	27,55	29,01
TiO ₂	0,05	0,04	0,03	0,06	0,77	0,18	0,21	0,06	0,15
Al ₂ O ₃	16,35	16,19	16,31	19,32	18,53	18,46	19,63	19,05	19,05
FeOt	18,48	14,92	13,89	22,73	21,88	19,65	22,95	25,72	25,95
MnO	0,20	0,16	0,20	0,65	0,40	0,12	0,74	0,35	0,20
MgO	19,94	20,13	19,78	17,21	17,27	18,71	17,33	15,54	14,55
CaO	0,09	0,12	0,02	0,03	0,29	0,07	0,05	0,06	0,03
Na ₂ O	0,09	0,04	0,02	0,03	0,03	0,05	0,00	0,02	0,02
K ₂ O	0,05	0,10	0,08	0,07	0,04	0,09	0,04	0,04	0,26
Total	82,66	79,01	77,50	89,07	87,92	88,40	89,74	88,39	89,22
Si	2,97	3,03	3,05	2,95	2,95	3,12	2,91	2,88	2,99
Al ^{IV}	1,03	0,97	0,95	1,05	1,05	0,88	1,09	1,12	1,01
Al ^{VI}	1,05	1,14	1,21	1,27	1,20	1,30	1,26	1,23	1,31
Ti	0,00	0,00	0,00	0,00	0,06	0,01	0,02	0,00	0,01
Fe ²⁺	1,67	1,38	1,30	1,94	1,88	1,65	1,94	2,25	2,24
Mg	3,22	3,32	3,31	2,61	2,65	2,80	2,61	2,42	2,24
Mn	0,02	0,01	0,02	0,06	0,04	0,01	0,06	0,03	0,02
Ca	0,01	0,01	0,00	0,00	0,03	0,01	0,01	0,01	0,00
Na	0,02	0,01	0,00	0,01	0,01	0,01	0,00	0,00	0,00
K	0,01	0,01	0,01	0,01	0,01	0,01	0,01	0,01	0,03
Σ oct	5,94	5,84	5,83	5,82	5,73	5,74	5,81	5,90	5,79
Fe/(Fe+Mg)	0,34	0,29	0,28	0,43	0,42	0,37	0,43	0,48	0,50

Table 3

	Chlorite in the illitic zone						
SiO ₂ (Wt %)	27,65	26,27	26,40	26,18	25,47	26,38	27,97
TiO ₂	2,05	2,10	1,83	1,35	0,03	0,04	0,19
Al ₂ O ₃	15,62	15,58	15,85	15,51	17,79	18,77	21,39
FeOt	31,22	31,48	29,90	32,43	31,55	29,70	34,02
MnO	0,34	0,21	0,46	0,40	0,42	0,37	0,16
MgO	10,27	10,70	10,44	10,18	10,57	10,79	5,82
CaO	0,08	0,07	0,09	0,13	0,06	0,03	0,02
Na ₂ O	0,05	0,02	0,07	0,04	0,06	0,01	0,00
K ₂ O	0,20	0,13	0,15	0,44	0,33	0,64	0,91
Total	87,48	86,55	85,18	86,65	86,29	86,73	90,47
Si	3,02	2,92	2,96	2,93	2,85	2,89	2,87
Al ^{IV}	0,98	1,08	1,04	1,07	1,15	1,11	1,13
Al ^{VI}	1,04	0,96	1,05	0,98	1,19	1,32	1,47
Ti	0,17	0,18	0,15	0,11	0,00	0,00	0,02
Fe ²⁺	2,86	2,93	2,80	3,04	2,95	2,72	3,22
Mg	1,67	1,77	1,74	1,70	1,76	1,76	1,03
Mn	0,03	0,02	0,04	0,04	0,04	0,03	0,03
Ca	0,01	0,01	0,01	0,01	0,01	0,00	0,00
Na	0,01	0,00	0,02	0,01	0,01	0,00	0,06
K	0,03	0,02	0,02	0,06	0,05	0,09	0,06
Σ oct	5,57	5,66	5,60	5,72	5,90	5,80	5,72
Fe/(Fe+Mg)	0,63	0,62	0,62	0,64	0,63	0,61	0,76

Table 4

	Phengite								
SiO ₂ (Wt %)	48,54	46,16	46,05	47,05	50,79	46,02	47,94	47,29	47,42
TiO ₂	0,09	0,09	0,12	0,15	0,08	0,10	0,02	0,10	0,13
Al ₂ O ₃	26,03	26,84	26,90	25,19	27,04	26,45	28,16	26,72	27,89
FeOt	5,09	5,72	5,43	5,14	4,38	5,99	4,45	5,03	4,67
MnO	0,03	0,08	0,03	0,03	0,12	0,12	0,01	0,05	0,02
MgO	2,07	2,09	1,94	1,79	2,62	1,89	1,97	2,01	1,91
CaO	0,05	0,02	0,09	0,12	0,15	0,04	0,04	0,00	0,05
Na ₂ O	0,06	0,03	0,08	0,25	0,07	0,12	0,09	0,03	0,09
K ₂ O	10,15	10,14	9,90	9,46	9,91	10,24	10,60	10,57	10,78
Total	92,10	91,17	90,54	89,16	95,15	90,97	93,29	91,79	92,96
Si	3,36	3,25	3,26	3,36	3,38	3,26	3,28	3,30	3,27
Al ^{IV}	0,64	0,75	0,74	0,64	0,62	0,74	0,72	0,70	0,73
Al ^{VI}	1,49	1,48	1,50	1,49	1,51	1,47	1,55	1,50	1,54
Ti	0,00	0,00	0,01	0,01	0,00	0,01	0,00	0,01	0,01
Fe ²⁺	0,27	0,30	0,29	0,28	0,22	0,32	0,23	0,26	0,24
Mg	0,21	0,22	0,20	0,19	0,26	0,20	0,20	0,21	0,20
Mn	0,00	0,00	0,00	0,00	0,01	0,01	0,00	0,00	0,00
Ca	0,00	0,00	0,01	0,01	0,01	0,00	0,00	0,00	0,00
Na	0,01	0,00	0,01	0,03	0,01	0,02	0,01	0,00	0,01
K	0,90	0,91	0,89	0,86	0,84	0,92	0,93	0,94	0,95
Inter Charg	0,91	0,92	0,91	0,91	0,86	0,94	0,94	0,95	0,96
Σ oct	1,97	2,00	2,00	1,95	1,99	1,99	1,99	1,98	1,98
Fe/(Fe+Mg)	0,55	0,58	0,59	0,59	0,46	0,61	0,53	0,56	0,55

Table 5

	Illite							
SiO ₂ (Wt %)	53,18	48,09	52,96	48,03	47,47	52,21	53,30	48,89
TiO ₂	0,29	0,08	0,09	0,05	0,01	0,09	0,11	0,14
Al ₂ O ₃	35,37	34,46	36,45	34,06	32,50	36,27	36,23	32,59
Fe2O3	2,73	1,07	1,81	1,29	1,91	1,83	1,81	1,09
MnO	0,04	0,01	0,00	0,00	0,00	0,04	0,04	0,00
MgO	1,02	0,66	0,69	0,83	0,52	0,55	0,83	1,49
CaO	0,03	0,05	0,04	0,06	0,18	0,04	0,03	0,08
Na ₂ O	0,08	0,14	0,08	0,12	0,07	0,08	0,07	0,11
K ₂ O	9,51	9,54	9,37	9,81	8,74	9,45	9,40	9,94
Total	102,25	94,08	101,48	94,25	91,40	100,55	101,81	94,32
Si	3,25	3,19	3,24	3,19	3,24	3,23	3,25	3,25
Al IV	0,75	0,81	0,76	0,81	0,76	0,77	0,75	0,75
Al VI	1,79	1,89	1,87	1,86	1,85	1,88	1,86	1,80
Ti	0,01	0,00	0,00	0,00	0,00	0,00	0,01	0,01
Fe ²⁺	0,13	0,05	0,08	0,06	0,10	0,09	0,08	0,05
Mg	0,09	0,06	0,06	0,08	0,05	0,05	0,08	0,15
Mn	0,00	0,00	0,00	0,00	0,00	0,00	0,00	0,00
Ca	0,00	0,00	0,00	0,00	0,01	0,00	0,00	0,01
Na	0,01	0,02	0,01	0,01	0,01	0,01	0,01	0,01
K	0,74	0,81	0,73	0,83	0,76	0,75	0,73	0,84
Inter Charg	0,75	0,83	0,74	0,84	0,78	0,76	0,74	0,86
Σ oct	2,01	2,01	2,02	2,01	2,00	2,01	2,02	2,00
Fe/(Fe+Mg)	0,58	0,65	0,57	0,59	0,76	0,63	0,52	0,58

Table 6

	Epidote					Allanite							
Na ₂ O (Wt %)	0,10	0,15	0,10	0,04	0,00	0,06	0,04	0,10	0,04	0,03	0,02	0,08	0,04
MgO	0,00	0,01	0,11	0,01	0,18	0,22	0,16	0,12	0,44	0,28	0,80	0,12	0,25
Al ₂ O ₃	19,84	21,31	19,26	21,06	22,08	13,59	13,69	13,65	13,19	14,56	17,23	15,82	18,27
SiO ₂	34,15	36,96	32,96	35,67	37,94	28,98	30,00	29,06	28,79	28,03	32,56	28,11	33,05
K ₂ O	0,05	0,11	0,03	0,04	0,01	0,08	0,04	0,06	0,10	0,03	0,03	0,06	0,03
CaO	20,28	21,00	20,58	21,65	21,46	10,15	10,74	10,64	12,00	10,45	11,03	11,11	11,30
TiO ₂	0,11	0,07	0,04	0,04	0,45	0,23	0,44	0,47	1,70	0,22	0,64	0,24	0,13
MnO	0,00	0,06	0,02	0,12	14,74	0,20	0,33	0,13	0,14	0,22	0,24	0,48	0,62
FeOt	14,34	14,39	14,68	14,23	0,01	15,25	15,48	14,41	14,45	12,26	12,40	10,76	12,01
Nd ₂ O ₃	0,00	0,00	0,16	0,00	0,36	3,07	1,79	1,03	1,34	3,15	3,25	1,48	2,83
Ce ₂ O ₃	0,32	0,15	0,20	0,90	0,00	10,11	9,82	9,55	9,87	10,91	10,37	9,84	9,23
La ₂ O ₃	0,38	0,13	0,27	0,00	0,09	6,67	6,04	5,80	4,41	5,92	5,70	5,52	5,40
Total	89,57	94,33	88,42	93,76	97,32	88,61	88,56	85,03	86,46	86,06	94,26	83,64	93,16
Si	2,99	3,05	2,95	2,99	3,03	2,95	3,00	3,01	2,94	2,93	3,01	2,95	3,05
Al	2,05	2,07	2,03	2,08	2,08	1,63	1,62	1,67	1,59	1,79	1,88	1,96	1,99
Ti	0,01	0,00	0,00	0,00	0,03	0,02	0,03	0,04	0,13	0,02	0,04	0,02	0,01
Mn	0,00	0,00	0,00	0,01	0,00	0,02	0,03	0,01	0,01	0,02	0,02	0,04	0,05
Fe ²⁺	0,94	0,89	0,99	0,90	0,89	1,17	1,17	1,12	1,11	0,97	0,86	0,85	0,83
Mg	0,00	0,00	0,01	0,00	0,02	0,03	0,02	0,02	0,07	0,04	0,11	0,02	0,03
Ca	1,90	1,86	1,98	1,94	1,84	1,11	1,15	1,18	1,31	1,17	1,09	1,25	1,12
Na	0,02	0,02	0,02	0,01	0,00	0,01	0,01	0,02	0,01	0,01	0,00	0,02	0,01
K	0,01	0,01	0,00	0,00	0,00	0,01	0,00	0,01	0,01	0,00	0,00	0,01	0,00
Nd	0,00	0,00	0,01	0,00	0,01	0,16	0,09	0,06	0,07	0,17	0,15	0,08	0,13
Ce	0,01	0,00	0,01	0,03	0,00	0,38	0,36	0,36	0,37	0,42	0,35	0,38	0,31
La	0,01	0,00	0,01	0,00	0,00	0,25	0,22	0,22	0,17	0,23	0,19	0,21	0,18
Fe/(Fe+Al)	0,32	0,30	0,33	0,30	0,30	0,42	0,42	0,40	0,41	0,35	0,31	0,30	0,30

Table 7

	Monazite (KA6 437,85)				Monazite (GR1 631)			
SiO ₂ (Wt %)	0,37	1,22	0,39	0,43	0,88	0,22	0,72	0,42
P ₂ O ₅	30,73	29,76	30,99	30,76	30,13	28,66	29,55	29,66
CaO	1,14	1,37	1,12	1,18	0,28	0,25	0,28	0,20
Y ₂ O ₃	0,97	0,90	0,99	1,04	0,74	0,79	0,68	0,59
La ₂ O ₃	15,05	14,98	15,61	15,63	18,74	18,17	17,30	20,10
Ce ₂ O ₃	30,47	29,80	30,31	30,07	33,50	33,26	33,76	33,16
Pr ₂ O ₃	2,99	2,92	2,95	3,04	3,54	3,88	3,33	3,21
Nd ₂ O ₃	13,10	11,93	12,42	12,01	8,20	8,76	8,30	7,32
Sm ₂ O ₃	1,40	1,65	1,51	1,65	0,59	0,67	0,37	0,59
Gd ₂ O ₃	0,72	0,69	0,63	0,79	0,37	0,79	0,47	0,08
PbO	0,05	0,13	0,08	0,09	0,02	0,02	0,04	0,00
ThO ₂	0,87	1,33	0,72	0,96	0,03	0,00	0,01	0,01
UO ₂	0,01	0,01	0,00	0,02	0,01	0,09	0,04	0,01
Total	97,46	96,27	97,29	97,22	97,04	95,57	94,85	95,36
Th/La	0,06	0,09	0,05	0,06	0,00	0,00	0,00	0,00
ΣREE	64,71	62,86	64,42	64,23	65,68	66,32	64,20	65,07

Table 8

Pb ppm	Th ppm	U ppm	Th/U	2 sigma error		2 sigma error		Age (Ma)	2 sigma error		
				Pb207/U23Pb207/U23Pb206/U23Pb206/U23					Pb207/Pb2 Pb207/Pb2	06	
				5	5	8	8				
473	5291	42	125	10,43	0,51	0,35	0,01	0,76	2949	76	
525	6228	56	112	7,68	0,33	0,26	0,01	0,82	2956	64	
370	4400	34	131	10,04	0,56	0,32	0,01	0,72	3031	89	
341	3703	29	126	10,77	0,55	0,35	0,01	0,75	3001	79	
415	4816	45	107	9,56	0,46	0,31	0,01	0,77	2997	74	
580	6964	60	116	10,14	0,45	0,33	0,01	0,81	3026	67	
507	5934	59	100	8,48	0,44	0,27	0,01	0,74	3016	82	
316	2877	32	89	9,73	0,45	0,31	0,01	0,79	3032	71	
384	4442	48	92	7,21	0,41	0,24	0,01	0,70	2993	91	
			-						-	-	
558	7279	65	112	5,43	0,44	0,22	0,01	0,58	2640	138	
786	10178	125	82	3,43	0,21	0,14	0,01	0,65	2598	102	
861	10420	84	124	6,10	0,28	0,25	0,01	0,77	2610	73	
680	7568	60	126	6,95	0,33	0,29	0,01	0,76	2618	75	
740	8807	81	109	6,24	0,28	0,27	0,01	0,77	2542	72	
303	3611	50	72	4,15	0,25	0,17	0,01	0,65	2622	100	
509	7707	138	56	3,29	0,17	0,14	0,01	0,72	2559	82	
273	3438	42	81	4,97	0,30	0,20	0,01	0,66	2658	99	
296	3850	66	59	4,34	0,24	0,18	0,01	0,68	2648	92	
345	4850	82	59	3,37	0,19	0,14	0,01	0,67	2599	93	
676	7159	61	118	9,49	0,44	0,40	0,01	0,78	2584	72	
391	3131	23	136	13,20	0,68	0,52	0,02	0,73	2698	82	
283	1741	24	72	9,19	0,58	0,37	0,02	0,65	2642	104	
798	9406	68	139	8,30	0,37	0,32	0,01	0,80	2705	68	
748	11219	117	96	5,68	0,24	0,18	0,01	0,83	3049	63	
738	11372	122	93	4,90	0,23	0,17	0,01	0,77	2924	74	
735	10807	118	91	4,97	0,22	0,17	0,01	0,80	2878	67	
780	11614	99	117	5,89	0,26	0,20	0,01	0,80	2916	67	
669	8923	63	142	8,68	0,39	0,29	0,01	0,80	2975	67	
631	8724	66	132	7,70	0,33	0,25	0,01	0,81	3009	65	
631	8254	56	146	7,38	0,36	0,27	0,01	0,75	2841	77	
736	9649	62	157	7,75	0,35	0,26	0,01	0,79	2930	69	
597	7892	52	152	6,15	0,31	0,21	0,01	0,74	2942	80	
490	6660	56	119	4,86	0,26	0,16	0,01	0,72	2936	84	
707	9391	60	156	6,69	0,31	0,23	0,01	0,78	2920	71	
754	10964	88	125	6,61	0,30	0,25	0,01	0,79	2780	69	
680	9151	81	114	5,40	0,26	0,23	0,01	0,73	2576	78	
736	9140	61	151	8,32	0,38	0,32	0,01	0,78	2733	71	
622	7734	60	128	6,51	0,32	0,23	0,01	0,74	2891	78	
450	5431	38	145	10,28	0,49	0,36	0,01	0,76	2865	73	
555	6692	50	135	10,38	0,48	0,36	0,01	0,77	2912	72	
606	7235	40	180	10,74	0,52	0,37	0,01	0,76	2927	75	
556	6780	64	106	8,36	0,37	0,28	0,01	0,79	2941	67	
352	2909	36	81	7,49	0,46	0,30	0,01	0,65	2658	101	

Table 9

GR1-631 Analysis					2 sigma error		2 sigma error		Age (Ma)	2 sigma error	
	Pb ppm	Th ppm	U ppm	Th/U	Pb207/U235	Pb207/U235	Pb206/U238	Pb206/U238	Rho	Pb207/Pb206	Pb207/Pb206
05120912c	231	1429	337	4,2	5,78	0,24	0,35	0,01	0,85	1976	63
06120912c	143	582	316	1,8	5,38	0,24	0,33	0,01	0,78	1931	73
07120912c	265	1799	399	4,5	5,51	0,22	0,33	0,01	0,87	1948	60
08120912c	191	1387	199	7,0	7,69	0,35	0,36	0,01	0,78	2401	70
17120912c	72	31	224	0,1	6,03	0,31	0,35	0,01	0,68	2037	86
18120912c	125	442	264	1,7	6,49	0,36	0,35	0,01	0,65	2157	92
19120912c	96	77	303	0,3	5,87	0,32	0,34	0,01	0,66	2057	90
20120912c	158	234	466	0,5	5,78	0,31	0,34	0,01	0,66	1993	90
21120912c	133	25	301	0,1	10,97	0,60	0,38	0,01	0,66	2917	84
22120912c	322	2263	294	7,7	10,03	0,56	0,38	0,01	0,64	2760	88
23120912c	363	1934	359	5,4	14,02	0,79	0,41	0,01	0,64	3161	86

Table 10

Sample	$\delta^{18}\text{O}$ (‰ SMOW)	$\delta^{13}\text{C}$ (‰ PDB)
GR5-510	11,5	-5,33
GR23-630,9	10,5	-13,76
GR23-631,5	10,9	-9,56
GR43-636	10,4	-7,02
GR43-638	10,2	-6,80
KA6-462	17,7	-10,65